# Optimization of a combined power plant $CO_2$ capture and direct air capture concept for flexible power plant operation †

Edward J. Graham,[a] Moataz Sheha,[a] Dharik S. Mallapragada,[a*] Howard J. Herzog,[a] Emre Gençer,[a] Phillip Cross,[b] James Custer,[b] Adam Goff,[b] Ian Cormier,[b]

The cost-effective integration of variable renewable energy (VRE) generation is critical for power sector decarbonization but is contingent on designing power systems to be more flexible. Deployment of carbon capture and storage (CCS) equipped fossil fuel power plants on the supply-side and direct air capture (DAC) technologies on the demand side can address the dual challenge of lower carbon emissions while providing grid flexibility. Historically, these two technologies have been contemplated for independent deployment where challenges related to high capital cost and flexible operation remain barriers. In this work, we consider the design and operations optimization of a flexible natural gas power plant concept with the potential for negative emissions that integrates three technologies: calcium looping, membrane and cryogenic $CO_2$ separation, and DAC. Global optimization using surrogate modeling approaches is performed to determine the optimal design and scheduling of the process with respect to different time varying electricity profiles, carbon price scenarios and fuel price scenarios expected in a high VRE penetration electricity grid. In general, we find that positive net present values are achievable for the negative emissions power plant concept while retaining flexibility of the power plant and high capacity utilization of all $CO_2$ capture related units, if the carbon price is at or above \$150/tonne. At these carbon price scenarios, which are in the range of available policy credits for DAC in some regions (e.g. U.S.) as of 2021, we also substantiate the synergistic integration of the proposed concept, where: a) the proposed process results in 52% higher NPV vs. a standalone calcium looping + DAC system and b) 7% higher NPV, 3% higher negative emissions and 2% higher net power production vs. a decoupled process where the natural gas power plant flue gas is not used within the calcium looping + DAC system.

## 1 Introduction

Economy-wide decarbonization efforts are expected to heavily rely on wind and solar-based electricity generation to reduce $CO_2$ emissions from the electric power sector as well as widespread electrification of many end-uses across transport, buildings and industry[1,2]. Both these strategies will increase the spatial and temporal variability in electricity supply and demand that complicates system operations and requires enabling technologies to ensure cost-effective, low-carbon and reliable electricity supply. Recent studies evaluating deep decarbonization of power systems[3–6] highlight the importance of relying on a broad suite of supply and demand-side technologies to provide flexibile system balancing and complement the low-marginal cost and intermittent nature of variable renewable energy (VRE) generation. On the supply side, this could include deployment of short and long-duration energy storage technologies, network expansion as well as deployment of firm low-carbon generation resources, such as carbon capture and storage (CCS) equipped fossil fuel power plants. On the demand-side, the deployment of distributed energy resources, demand flexibility and energy efficiency measures can be complemented by technologies capable of using electricity to reduce atmospheric $CO_2$ emissions like direct capture (DAC). Here, we evaluate the cost-effective design and operation of a power plant concept that combines flue gas $CO_2$ capture with a DAC process in a way that enables flexible operation and negative emissions generation when integrated into a VRE-dominant power grid.

In general, integrating $CO_2$ capture systems with a natural gas (NG) power plant changes power plant operating behavior by: a) reducing plant energy efficiency due to energy consumption for $CO_2$ capture[7,8] and b) potentially limiting ability of the plant to adjust its output to respond to market signals, due to limited operational flexibility of $CO_2$ capture systems and their often tight thermal coupling with power generation equipment[9]. For instance, the state-of-the-art (SOA) $CO_2$ capture approach based on amine-scrubbing is known to reduce power plant flexibility[10], and generally captures only 90% of the $CO_2$ emissions. The design of flexible CCS-equipped fossil fuel power plants is therefore an important area of current research, whereby the capture system reacts to changes in the dispatch of the power plant (and consequently, inlet flue gas flow rate), and flexible operation leverages the variability in the electricity price to maximize profit. Typical methods proposed to facilitate flexible operation in the case of amine-based $CO_2$ capture processes include solvent storage, exhaust gas venting (decoupling energy generation from $CO_2$ capture at peak electricity prices), and time-varying solvent regeneration (accumulating $CO_2$ in the solvent at peak electricity prices)[11–14].

The challenges of designing flexible CCS-based power generation schemes makes it interesting to consider DAC systems that, in principle, allow for separating the $CO_2$ capture step and dispatchable power generation step across both space and time. As a standalone system, DAC could be operated in a baseload manner to utilize electricity from the grid to capture atmospheric $CO_2$. In turn, the captured $CO_2$ can be used to offset emissions from flexible and sparing operation of NG power plants in a VRE-dominant grid, and effectively achieve the same overall emissions outcomes. A major drawback of this approach, however, is that the $CO_2$ is

* Corresponding author, [a] *MIT Energy Initiative, Massachusetts Institute of Technology, Cambridge, MA, USA. E-mail: dharik@mit.edu*
[b] *8 Rivers Capital, Durham, USA*

captured from a source with two orders of magnitude lower $CO_2$ concentration than the flue gas exhaust of a modern NG combined cycle power plant (around 400 ppm vs. 4 vol% $CO_2$ concentration), which is likely to substantially increase the cost of $CO_2$ capture.

Here we explore the potential to integrate the DAC and power plant $CO_2$ capture processes in a way that allows for balancing cost of $CO_2$ capture while maintaining flexible power plant operations. Figure 1a summarizes one manifestation of the concept, that combines commercially available Ca-looping technology and electricity based $CO_2$ purification processes with emerging processes for lime-based DAC. The calcium loop is used separate $CO_2$ from the power plant flue gas exhaust, with CaO being the chemical sorbent, that has a relatively low energy penalty of $CO_2$ capture and is a cheaper sorbent compared to alkanolamines. The calciner produces CaO, which can be used in the DAC process (named Calcite) to capture $CO_2$ from the atmosphere in a semi-batch manner with use of intermediate solid storage to maximize DAC capacity utilization. The $O_2$ composition in the feed gases to the calciner is limited to below 30%, which enables the use of air-fired rotary kilns that are readily available at the current time and allows for the use of power plant flue gas as a primary source of $O_2$ for combustion. Prior to sending it to DAC, CaO from the calciner is cycled a few times to capture $CO_2$ from the process streams, which have a relatively high $CO_2$ composition compared to air, in the carbonator at high temperatures ($\approx$ 600C). The calciner off-gas, which contains $CO_2$ from flue gas, natural gas combustion and feed limestone, has a relatively high concentration (>30%) and thus can be purified via electrically-driven membrane and cryogenic separation units to produce a high purity liquid suitable for sequestration and a vent gas stream that may be recycled for additional $CO_2$ recovery. The major process units (DAC, calciner and separation system) in Figure 1 can operate continuously to handle the feed $CaCO_3$ even at zero NGCC plant loadings, meaning that the process can operate flexibly in response to variations in the flue gas feed. The unit operations for $CO_2$ separation and purification rely on electricity rather than heat (via steam) as the primary energy input, which enables fully decoupling the $CO_2$ capture stage from the power plant operations. This is in contrast to amine-based $CO_2$ capture, where steam for amine regeneration is generally sourced from the Rankine cycle for power generation to maximize overall system efficiency. The advantages of using Ca-looping technology over the conventional alkanolamine-based processes are the relatively low energy penalty and relatively cheap sorbent. Finally, another advantage of integrating calcium looping with DAC is that lime hydration reverses sorption degradation that is known to occur with repeated looping[15], allowing for high CaO conversions within the DAC system independent of CaO degradation within the calcium loop. To our knowledge, although there are several studies that have theorized processes to integrate cement production and a power generation via a Ca-looping process for $CO_2$ capture[16–18], no studies have considered the integration of DAC and power plant $CO_2$ capture under dynamic power plant operation in response to VRE dominant grids.

The process of Figure 1 involves several potential heat and mass interaction between different unit operations that can be optimized to maximize profitability while simultaneously considering the effect of these interactions on the dynamic operation of the power plant in response to volatile electricity prices. Although there is extensive literature on techno-economic analysis of amine-based $CO_2$ capture at power plants, several studies focus on analysis under steady-state plant operation[19,20] which ignores the techno-economic impact of increased power plant cycling in grids dominated by VRE generation and rapidly changing electricity prices. Other techno-economic assessments of CCS-equipped power plants rely on a multi-period optimization approach to study the cost implications of flexible operation of various units as well as sizing decisions related to $CO_2$ capture and power generation equipment under various electricity price, $CO_2$ price and fuel price scenarios[12,21–23]. Here, a common approach involves formulating an optimization model that evaluates operations over multiple time periods over the year with a given set of electricity prices to maximize profits. Zantye et al.[13] conducted profit maximization on a flexible monoethanolamine-based carbon capture process, and considered uncertainty in the hourly electricity prices by formulating a multi-stage stochastic optimization problem. To balance accuracy against computational tractability, these studies and others focused on design of fuel production processes using electricity[24–26], make several approximations such as: a) considering only a subset of design considerations as model decision variables[12,23], b) simplified representation of operational dynamics of each unit in the process[12,22,26], c) limiting number of operational periods evaluated within the optimization model[21,27] and d) developing surrogate models to reduce the computational complexity of the equations present in the optimization problem[13]. To date, nearly all but one[23] of the techno-economic studies on flexible CCS plant operations have focused on studying solvent-based $CO_2$ capture processes and generally involve fewer design degrees of freedom as compared to the process of Figure 1.

In this work we evaluate the optimal plant design and operational schedule of the proposed negative-emissions power plant concept with respect to different market scenarios[28,29] corresponding to different combinations of natural gas prices, electricity price profiles and carbon prices, adapted from a recent U.S. department of energy research program on flexible carbon capture[30]. Our analysis is based on developing a generalized design and scheduling based optimization framework that balances accuracy with computational tractability by incorporating: a) nonlinear cost and performance characterization of key unit operations via developing surrogate models b) consideration of alternative process integration schemes via a superstructure representation approach using binary variables and c) representation of temporal variability in electricity prices within the design optimization using a time-series clustering techniques. Through this framework, we find that the proposed negative-emissions power plant concept generally can achieve positive net present values under scenarios with carbon prices near or above \$150/tonne, with the role of DAC and negative emissions growing with carbon price. Importantly, the optimized system is shown to be capable to adapt to time-varying electricity prices via maximizing power

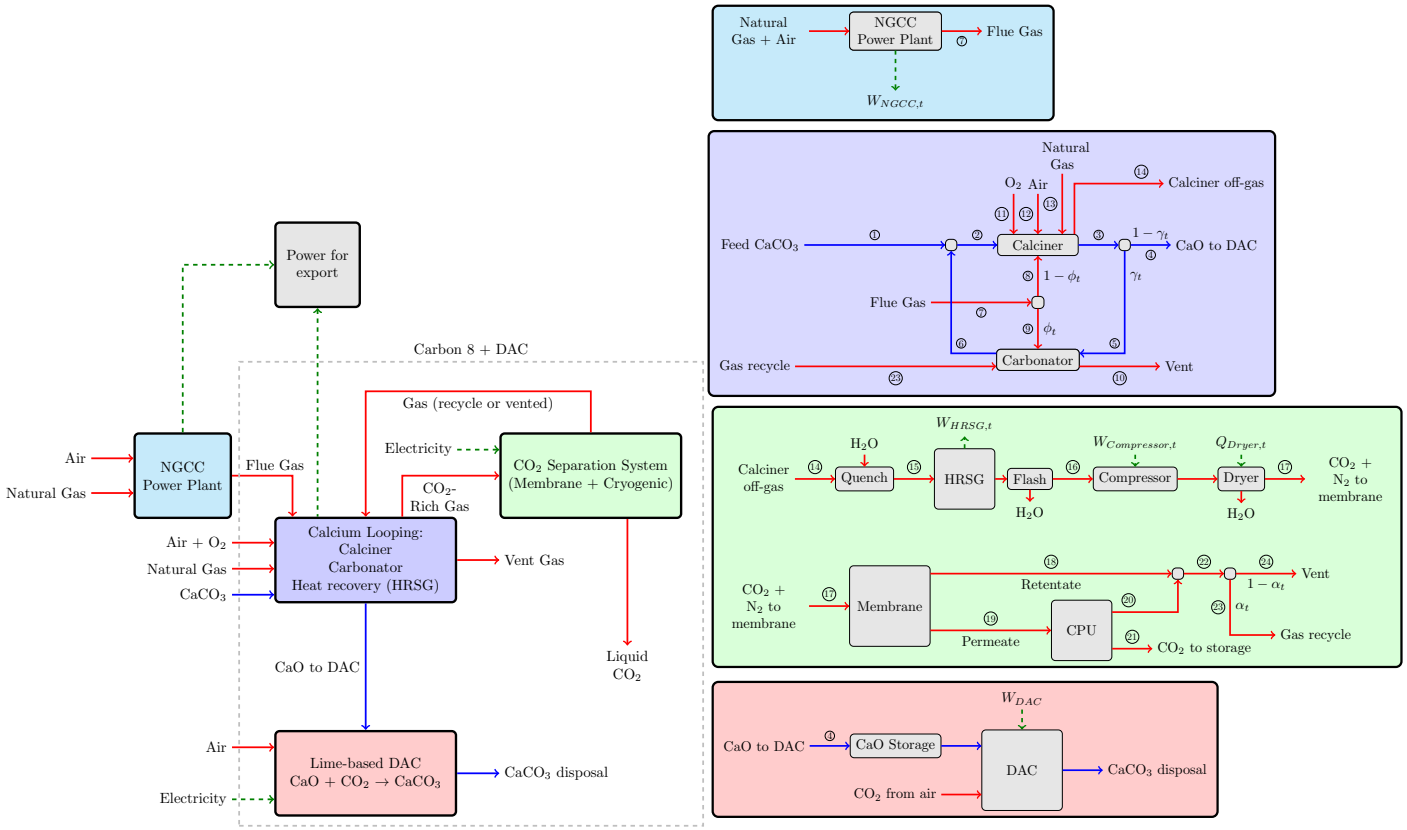


(a) Simplified process schematic.

(b) Detailed process schematic used within the optimization framework.

Fig. 1 Schematics illustrating the proposed concept for power plant $CO_2$ capture integrated with direct air capture. Blue lines refer to solid streams consisting of $CaCO_3$ and CaO, red lines refer to gaseous/ liquid streams, and green dashed lines refer to either movement of heat of electrical power. a) The process consists of an NGCC power plant that generates power from natural gas; a calcium looping system that captures $CO_2$ from the NGCC flue gas and recycled gases from the seperation system, and produces CaO for DAC; a lime based DAC system that captures $CO_2$ from the atmosphere; and a $CO_2$ separation system that captures high purity $CO_2$ at high pressure suitable for sequestration. The units within the grey dashed region are labelled 'Carbon 8 + DAC' as referred to throughout this work. b) In this schematic the major process units used within the optimization model described in this work are presented. Three important decision variables representing split fractions are shown in this figure: $\gamma_t$ is the fraction of calcined solids that are recycled to the carbonator vs DAC; $\phi_t$ is the fraction of NGCC gas solids sent to the carbonator vs the calciner; and $\alpha_t$ is the fraction of off-gases from the membrane and CPU units that are recycled to the carbonator.

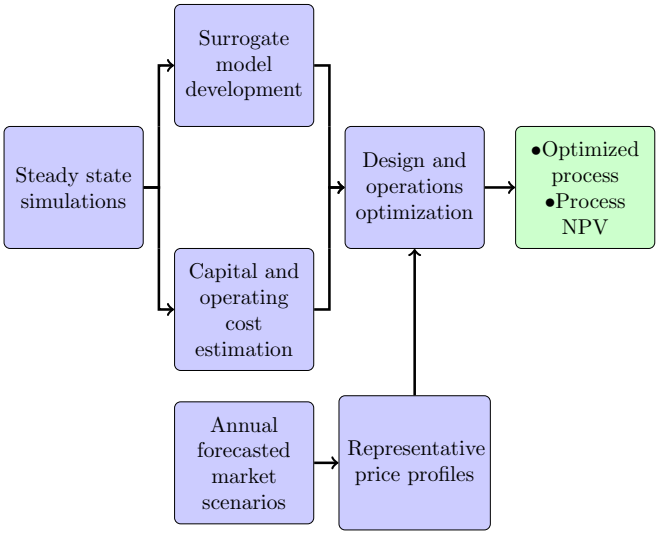


Fig. 2 Workflow schematic: Lines show the transfer of information between blocks. Using the steady state simulations in Aspen plus as a basis, surrogate models are developed, and capital and cost estimations are performed. Annual forecasted market scenarios are converted to representative electricity price profiles via k-means clustering. The surrogate models, cost models and representative price profiles are fed into a full design and operations optimization algorithm.

exports during times of high prices and becoming an net importer at times of low prices, all while maintaining high capacity utilization of the capital-intensive units downstream of the power plant. We also show the value of the synergistic integration between the DAC and $CO_2$ capture system wherein the combined process has greater NPV than the process where the flue gas from the NGCC plant is not used in the Ca-loop or the standalone DAC process.

The rest of the paper is structured as follows: Section 2 provides a description of the net-present value (NPV) maximization problem and the methods used in its construction, with details provided in the electronic supporting information (ESI). Section 2.5 summarizes specific implementation details for the optimization problem. Section 2.6 provides a description of the market scenarios developed as part of the ARPA-E FLECCS program. Section 3 presents the optimal design and operational schedule of the plant under the different market scenarios and different operational constraints. Finally, section 4 summarizes the overall work and highlights the key findings.

## 2 Methods

The design and scheduling optimization of the proposed process of Figure 1 relies on the steady-state modeling of the process conducted by Sheha *et al.* [31], who developed an Aspen simulation of the process and identified a number of key operational degrees of freedom for the process. The overall workflow is summarized in Figure 2, where details are each step are provided below and in the ESI.

### 2.1 Optimization model summary

Equation 1 summarizes the overall optimization model, where the objective is to maximize the project net present value ($NPV$) of the proposed flexible carbon capture process for a given market scenario $M$.

$$
\begin{aligned}
\max_{\mathbf{x}_t,\mathbf{y}_t,t\in\{1,\ldots,N_t\}} \quad & NPV(M) \\
\text{s.t.} \quad & NPV(M) = -CAPEX \\
& \quad + \frac{REVENUE_{annual}(M) - OPEX_{annual}(M)}{CRF} \\
& CAPEX = \sum_{u\in units} unitCost_u \\
& unitCost_u = a_u(capFlow_u) \quad u \in units \\
& capFlow_u \geq Flow_{u,t}(\boldsymbol{x}_t,\mathbf{y}_t) \quad t \in \{1,\ldots,N_t\}, u \in units \\
& f_t(\boldsymbol{x}_t,\mathbf{y}_t) = 0 \quad t \in \{1,\ldots,N_t\} \\
& g_t(\boldsymbol{x}_t,\mathbf{y}_t) \geq 0 \quad t \in \{1,\ldots,N_t\} \\
& \boldsymbol{x}_t^{lb} \leq \mathbf{x} \leq \boldsymbol{x}_t^{ub} \\
& \mathbf{y}_t \in \{0,1\} \quad t \in \{1,\ldots,N_t\},
\end{aligned}
\tag{1}
$$

where $M$ is the market scenario consisting of a yearly electricity price profile discretized in hours ($EP_t \quad t \in \{1,\ldots,N_t\}$), a fixed carbon price ($carbonPrice$) and fixed fuel price ($fuelPrice$), $CAPEX$ is the total capital cost of the plant, $REVENUE_{annual}(M)$ is the annualized revenue, $OPEX_{annual}(M)$ is the annualized operational expenditure, and $CRF$ is the capital recovery factor. $\mathbf{x}_t$ and $\mathbf{y}_t$ represent vectors of continuous variables (e.g., time-varying molar flowrates and split fractions) and binary variables respectively, indexed at time, $t$. $\boldsymbol{x}_t^{lb}$ and $\boldsymbol{x}_t^{ub}$ are lower and upper bounds on the continuous variables, respectively. Two binary variables related to power plant operation are considered, one represents the on/off operation of the NGCC plant and the other is used to estimate when the plant starts up (ref. ESI Section 1.1 ). Binary variables are also used implicitly within the piecewise linear approximation to the cost functions for each unit (ref. ESI equation S93). $CAPEX$ is computed as the sum of the cost of different sections of the plant, $unitCost_u$, where $u$ represents a system of aggregated process units (e.g., the DAC unit consists of a slaker, warehouse, materials handling, etc.). $unitCost_u$ is determined as a function $a_u$ of a capacity variable, $capFlow_u$, representing the maximum value of a particular operational variable (molar flowrate, power or inventory) associated with the unit operation throughout the year. $f_t$ and $g_t$ represent process equality and inequality constraints, respectively. These constraints describe: a) process topology, i.e. connections between unit operations and b) unit-level mass and energy balances and c)unit-level operational flexibility.

Process model constraints are described in ESI section S1. The constraints relating the decision variables with the various terms of the net present value $NPV$ objective are described in the ESI (section S2). Since the cost of each process unit can scale nonlinearly with respect to their corresponding capacity variables, a piecewise linear approximation is used to approximate the capi-

tal cost of each aggregated process unit as a function of its sizing variable, as described in ESI section S2.1. Figure 1b provides a more detailed schematic of the process model used within the optimization framework along with stream numbers.

### 2.2 Surrogate model for unit operations

For the purpose of global optimization, surrogate models are developed based on the detailed Aspen Plus model developed by Sheha *et al.*[31] to describe unit-level operational constraints. In most cases, linear correlations are developed based on sensitivity analyses on the Aspen Plus model (e.g., the relationship between the flowrate of flue gas exhaust from natural gas power plant and the feed natural gas flowrate is described by equation S4 in the ESI). As an example, for the membrane process unit (see section S5 of the ESI), reduced-order functions are generated using the ALAMO (Automated Learning of Algebraic Models) software[32]. The surrogate model is developed from the membrane model, which employs the cross-plug flow assumption and consists of a set of coupled ordinary differential equations. An adaptive sampling functionality is employed in order to avoid over-fitting of the model outputs. As illustrated in Figure 3, the reduced order model outputs regarding the mole fraction of $CO_2$ in the retentate and permeate streams ($y_{CO_2,ret}$ and $y_{CO_2,perm}$) and the stage cut ($\theta$) compare well against the outputs of the system of differential equations describing the unit, over a broad range of independent variables (feed pressure $P$, dimensionless area $\bar{\sigma}$ and feed $CO_2$ mole fraction $y_{CO_2,f}$). Moreover, the reduced-order models are quadratic in the independent variables (ESI equations S132 and S133) and are suitable for use within the global optimization problem due to their low numerical complexity.

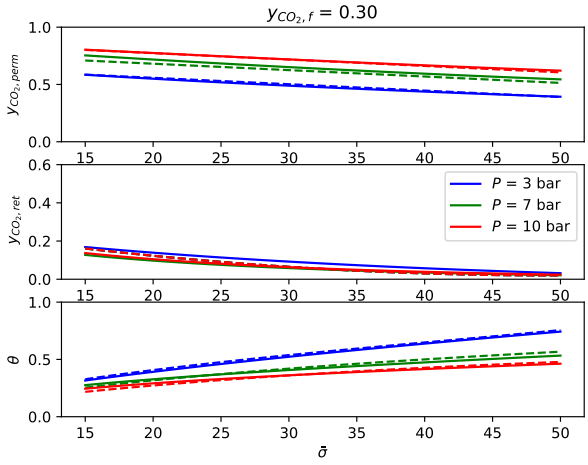


Fig. 3 Performance of the membrane surrogate model (dashed lines) with respect to the solution to the ordinary differential equation (ODE) model (continuous lines) at feed mole fraction $y_{CO_2,f} = 0.3$. $y_{CO_2,perm}$ is the mole fraction of $CO_2$ in the permeate, $y_{CO_2,ret}$ is the mole fraction of $CO_2$ in the retentate, $\theta$ is the stage cut, and $\bar{\sigma}$ is the dimensionless membrane area divided by the feed pressure. See ESI Section S5 for further details.

### 2.3 Modeling CaO degradation during Ca looping

As highlighted in the introduction, CaO degradation is an important phenomena to consider when modeling calcium looping processes. In section S3 of the ESI, we derive an analytic equation (ESI equation S118) for the conversion of CaO within the carbonator as a function of the solids split fraction $\gamma$, where $\gamma$ is the fraction of solids exiting the calciner that are sent to the carbonator (the other portion 1-$\gamma$ is sent to the direct air capture unit). This equation is developed based on experimental data[33] for a particular limestone source and particle size. In ESI Figure S2 we show how the average CaO conversion decreases nonlinearly with $\gamma$.

### 2.4 Model temporal reduction

To reduce the number of operational time periods to be modeled to capture time-varying electricity prices, we model plant operations over representative days at an hourly resolution. For each electricity price scenario evaluated, the representative days are sampled using a k-means clustering algorithm[34] that maps each day to a representative day. The methodology is described further in the ESI (section S4), where we also highlight how 30 representative days provide a good balance of accuracy and computational speed (see Figure S3 in the ESI). Example outputs from the k-means clustering algorithm applied to the electricity price profile in the MiNg $150 PJM and BaseCaseTax $60 market scenarios (explained in section 2.6) is shown in Figures S4 and S5 of the ESI, respectively. Notice that the representative day selected and weights for the representative day are unique to each electricity price scenario.

### 2.5 Implementation

The overall optimization problem (1) is a non-convex mixed-integer nonlinear program (MINLP), where all nonlinear terms in continuous variables are bilinear, and is solved to global optimality. The optimization problem is formulated in Pyomo[35,36], and Gurobi 9.5.2[37] is used as the global MINLP solver. Each optimization is run for 3 days on the MIT supercloud[38] using 48 Intel Xeon Platinum 8260 cores. The presolved model consists of 93589 constraints (of which 14400 are bilinear constraints), 37433 continuous variables and 1449 binary variables.

### 2.6 Overview of Market scenarios

We evaluate the optimal process design and economic outlook for various market scenarios developed as part of a flexible carbon capture research program managed by U.S Department of Energy (ARPA-E FLECCS *). As described elsewhere, the market scenarios were developed based on outputs from electricity sector capacity expansion models for different regional, technology and policy scenarios[28,29]. For example, one set of scenarios[28] labeled MiNg (mid natural gas price) consists of four energy market regions in the USA (CAISO, ERCOT, MISO-W, and PJM-W). A summary of the market scenarios evaluated in this work is presented in Table

* https://arpa-e.energy.gov/technologies/programs/fleccs

1. In general, these different tax scenarios are representative of different energy market regions in the USA. We assume that our process is a price-taker in the energy market, i.e., the electricity prices are independent of the net power produced or consumed by the system. The electricity price profiles across the market scenarios, representative of future VRE-dominant grids, present a significant challenge in operating natural gas power plants with CCS profitably since there are a large number of hours when the electricity price is zero, e.g., in the MiNg $150 ERCOT scenario the electricity price is approximately zero for 5178 out of 8760 hours (60%) of the year.

## 3 Results

In all results presented here, we fix the NGCC power plant capacity to be 740 MW ($W^{PP,CAP} = 0.74GW$, ref ESI Equations S2 and S3) and bound the calciner capacity to be less than or equal to the design flow rate considered in the steady-state Aspen simulation model (i.e. $capFlow^{max,calciner} \leq 17$ MMol/hr), described elsewhere [31]. These two assumptions ensure that the system does not reach infinite size at high carbon prices, and the flowrate is similar to that of a calcium looping system that does not produce CaO as a by-product [§]. In all cases apart from those presented in section 3.3, it is assumed that all flue gas enters the calcium loop (via either the calciner/ carbonator). This ensures that the capture system is always built if the NGCC is operational.

The results section is categorized as follows. In section 3.1, we describe results for the various market scenarios and explain how the elements of the market scenario affect the net present value of the project. In section 3.2, we isolate the impact of carbon prices on the model outcomes. Finally, in section 3.3, we quantify the synergy of coupling DAC and flue gas $CO_2$ capture, by comparing the economics of the coupled NGCC, Carbon 8 and DAC case with a case where NGCC flue gases are not incorporated into the calcium loop, and a case where the Carbon 8 and DAC system operates without an NGCC plant.

### 3.1 Forecasted market scenarios

The optimal process NPVs for the 14 market scenarios are presented in Table 1. The results indicate that the scenarios with relatively high fuel prices (2.94 $/MMBtu) and low carbon prices ($60/ton) result in the most negative NPVs, with a value of approximately -$2 bn. In particular, at $60/tonne carbon price, it would be more profitable to operate the NGCC without carbon capture (in this case, positive NPVs of approximately $0.9 bn would be achievable for the top four cases in Table 1). In contrast, positive NPVs are achievable in all cases where the carbon price is $150/tonne (MiNg $150 CAISO, MiNg $150 ERCOT, MiNg $150 NYISO and MiNg $150 PJM). This is promising since the 45Q enhancements in the US Inflation Reduction Act (IRA) [39] indicate that a $180/tonne credit is applied for storage in saline geologic formations from DAC.

To better understand the drivers of the process NPV, we developed a linear regression of the process NPV with respect to the carbon price, fuel price and average electricity price over the market scenarios shown in Table 1.

$$NPV(\$bn) = 0.043 carbonPrice(\$/tonne) - 0.267 fuelPrice(\$/MMBtu) + 0.032\bar{EP}(\$/MWh) - 5.66(\$bn), \quad (2)$$

with an $R^2$ value of 0.95 and standard deviation 0.43 $bn. $\bar{EP}$ is the average electricity price. This correlation provides a quantification of how the NPV changes with respect to key metrics computed for these specific scenarios. The carbon price coefficient is positive, indicating that the process is more profitable at higher carbon prices due to the increased revenue generated from negative emissions credits. The NPV decreases with natural gas price as expected. The NPV increases with the average electricity price due to greater revenues generated at times where the net power of the plant is positive.

### 3.2 Sensitivity on carbon price

To consider the effect of carbon price on the optimal process design and operation, we evaluated the model for additional set of scenarios where we fixed the electricity price profile and natural gas fuel price ($1.43/MMBtu) to the scenario of MiNg $150 PJM and only vary the carbon price (*carbonPrice*) between 60,100, and 150 $/tonne. In Figure 4a, the carbon balance on the overall system over yearly operation is shown. The relative proportion of sequestered $CO_2$ to $CO_2$ captured from the DAC unit at $150/tonne is 1.75, which is slightly above the range described in the DAC process developed by Carbon Engineering (1.3-1.5 t $CO_2$ sequestered per t $CO_2$ captured) [40]. As the carbon price increases, more $CO_2$ enters the process as natural gas, calcium carbonate, and atmospheric $CO_2$, while the amount of flue gas $CO_2$ entering the process decreases only slightly. In Figure 4b we show how the carbon price system influences the net power produced by the system in various electricity price bands. This illustrates that in general, power is produced when the electricity price is above $50/MWh, while it is consumed below $50/MWh. This cut-off price increases slightly with respect to the carbon price as reflected by the smaller amount of electricity generated in in the $50-$100/MWh price band. At higher carbon prices, more power is consumed at low electricity prices (between 0 and 50 $/MWh), and less power is produced at high electricity prices (above $50/MWh). This is due to the increased power requirement of the various process units when processing larger amounts of feed $CaCO_3$. Overall, it is clear that as the carbon price is increased from $ 60/tonne to $150/tonne, the optimal process design reduces emphasis on power generation in favor of generating negative emissions.

Figure 5 highlights the optimal plant dispatch at the different carbon prices, where we show operation of four days involving

§ The molar flowrate of $CO_2$ in the NGCC flue gas is 5.7 MMol/hr at full loading. Considering the case of infinite recycle, the CaO conversion approaches 0.25 as the number of cycles approaches infinity (ref. ESI equation S118 ) and thus the molar flow rate to the carbonator (and calciner) at infinite recycle would be approximately 22 MMol/hr, assuming that all flue gas is fed to the carbonator and 95% of the $CO_2$ is absorbed. Thus, the capacity bound of 17 MMol/hr is similar to what we would expect from a typical calcium looping process where CaO is not produced as a major by-product.

Table 1 Summary of market scenarios used in this work. Market scenarios are labeled with dollar values referring to the carbon price in $/tonne, # Zero EP refers to the number of hours in the year that the price is below $1/MWh (i.e., approximately zero). Rel. gap refers to the relative optimality gap at termination of the global optimization routine.

| Market Scenario | Fuel Price($/MMBtu) | Average EP ($/MWh) | #Zero EP (% Zero EP) | NPV ($bn) | Rel. Gap (%) |
|---|---|---|---|---|---|
| WinterNYTax $60 | 2.94 | 48.00 | 339 (3.9 %) | -2.24 | 1.92 |
| BaseCaseTax $60 | 2.94 | 47.69 | 791 (9.0 %) | -2.13 | 4.62 |
| HighSolarTax $60 | 2.94 | 45.43 | 1179 (13.5 %) | -2.11 | 5.14 |
| HighWindTax $60 | 2.94 | 45.06 | 1605 (18.3 %) | -2.08 | 4.49 |
| MiNg $100 ERCOT | 2.64 | 33.66 | 4048 (46.2 %) | -1.77 | 0.88 |
| MiNg $100 MISO-W | 1.69 | 35.12 | 3300 (37.7 %) | -1.10 | 1.29 |
| MiNg $100 PJM | 1.42 | 48.01 | 1352 (15.4 %) | -0.56 | 0.49 |
| MiNg $100 CAISO | 2.26 | 52.97 | 2167 (24.7 %) | -0.54 | 0.96 |
| MiNg $100 NYISO | 1.12 | 35.22 | 3161 (36.0 %) | -0.48 | 1.25 |
| MiNg $150 ERCOT | 2.64 | 36.18 | 5178 (59.1 %) | 1.06 | 3.14 |
| MiNg $150 MISO-W | 2.01 | 28.13 | 4560 (52.1 %) | 1.44 | 0.86 |
| MiNg $150 CAISO | 2.26 | 45.35 | 2963 (33.8 %) | 1.76 | 3.53 |
| MiNg $150 PJM | 1.43 | 49.81 | 2598 (29.7 %) | 1.97 | 0.19 |
| MiNg $150 NYISO | 1.14 | 33.67 | 4472 (51.1 %) | 2.26 | 2.01 |

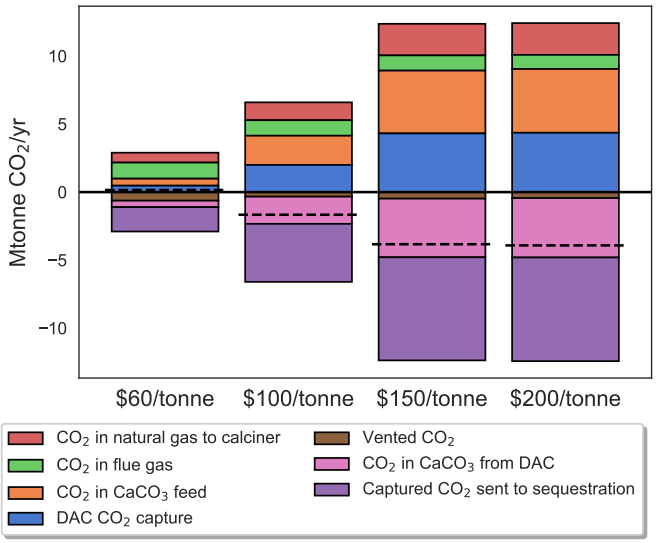


(a) Breakdown of $CO_2$ input (positive values) and output (negative values) to the process. NPV-optimal process under the MiNg $150 PJM market scenario with different carbon prices. The dashed black lines correspond to the net $CO_2$ emissions from the process (vented $CO_2$ - $CO_2$ captured by DAC).

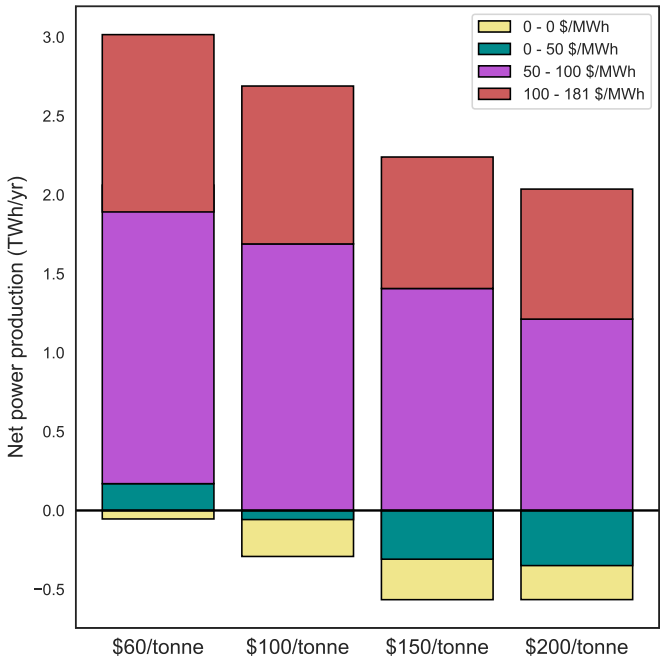


(b) Net power production of the overall system at various wholesale electricity price bands. The height of each colored block represents the power produced by the system if the block is above 0 on the $y$ axis, if the block is below 0 it represents the power consumed by the system at each price band. NPV-optimal process under the MiNg $150 PJM market scenario with different carbon prices.

Fig. 4 Breakdown of $CO_2$ sources and sinks, and net power production at different carbon prices.

periods of full- and part-loading of the NGCC plant. As expected, the NGCC plant is operational at high electricity prices, off at low electricity prices, and operates at part-load at intermediate electricity prices (shown by the blue region in the power production subplot). At lower carbon prices of \$60/tonne, the process power output varies from a maximum of 709 MW when the NGCC is operating at full capacity (740 MW) to a minimum of -13 MW when the NGCC is off. Thus, the $CO_2$ capture results in 4% reduction in power plant output, which is in a similar range compared to other calcium looping processes that do not produce a large amount of spent CaO as a byproduct (6-8%[41]). This relatively low energy penalty of $CO_2$ capture is due to the secondary source of power production in the HRSG after the calciner. Increasing the carbon price generally reduces the maximum power output and increases maximum power import by the process due to increasing deployment for DAC for negative emissions generation. Consequently, the net power ranges from 663 (10% reduction in nameplate NGCC output) to -63 MW for the \$100/tonne scenario and 609 MW (18% reduction vs. nameplate NGCC output) to -120 MW in the \$150/tonne scenario.

The subfigures labelled 'split fraction' in Figure 5 show the optimal time trajectories of three process decision variables: a) $\phi$ refers to the fraction of flue gas sent to the carbonator (the other portion 1-$\phi$ enters the calciner), b) $\gamma$ refers to the fraction of CaO exiting the calciner that is recycled to the carbonator (the other portion 1-$\gamma$ enters the DAC unit) and c) $\alpha$ refers to the fraction of gases exiting the membrane and cryogenic processing units that are recycled to the carbonator (the other portion 1-$\alpha$ is vented). In the \$100/tonne and \$150/tonne carbon price scenarios, it is optimal to send $\approx$ 80% of the flue gas to the carbonator, while the remaining 20% of the flue gas is used as a high-temperature source of oxidant in the calciner. As the carbon price increases, the feed $CaCO_3$ flowrate increases, driven by the increased negative emissions incentive. Thus, the extent of CaO recycling to the carbonator, reflected by $\gamma$, decreases with carbon price since a smaller proportion of CaO is required for $CO_2$ capture in the carbonator. This effect is compounded by the decreased degradation of CaO at lower recycle rates (see ESI Figure S2). In all cases, the recycled gases from the membrane and CPU units are vented at full NGCC loading. This contrasts with optimal operation results reported for power generation with flexible carbon capture processes that are not coupled with DAC (see e.g., [42]), when at high carbon prices it becomes necessary to capture residual $CO_2$ emissions. In this case, venting gases at full NGCC loading is more cost-effective than recycling them back to the carbonator since it reduces the overall CAPEX of the system, and it allows for a higher flowrate of CaO sent to the DAC unit, which offsets the emissions from vented $CO_2$. An additional benefit of venting the recycled gases at full NGCC loading and recycling at zero NGCC loading is that there is less time variation in the solid and gas flowrates to the carbonator (see solid flow rate panels in Figure 5). In section S7 of the ESI, we confirm that the NPV is lower when gases are recycled back to the carbonator during periods when the NGCC is off.

As shown in Figure 5 and ESI Figure S9, at carbon prices of \$150/tonne and above, the input solids to the calciner is constant and equal to the fixed upper bound on the input flowrate of 17 MMol/hr. The average capacity factors in the \$150/tonne scenario for the calciner, carbonator, CPU, limestone mill, HRSG and DAC are 99%, 75%, 98%, 87%, 97% and 100% respectively over the yearly operation. Such high capacity factors are encouraging from a capital utilization perspective, since all units excluding the NGCC can be run continually regardless of the NGCC loading, with only small variations in unit operation. This is in contrast to the standard approaches to calcium looping operation that are typically load-following[43]. Looking at gas flow rates panel in Figure 5, we see that, at \$100/tonne and \$150/tonne carbon prices, flue gas to the calciner is substituted for air when the NGCC turns off, and the oxygen stream from the VPSA is generated such that the inequality constraint on the maximum allowed oxygen concentration (0.3 mole fraction, ref. ESI equation S37) of oxygen is binding at all times. This may imply that the process would be more profitable if the calciner design allowed for higher oxygen concentrations in the feed, thus reducing the cost of the downstream separation units.

Figure 6b highlights the capital cost (CAPEX) and operating cost (OPEX) breakdown of the optimal process at different carbon prices, where it is clear that the calciner, NGCC plant, DAC, VPSA and compression before the membrane unit are the largest contributors to the total CAPEX under profitable operation. In general, the cost of each unit increases with carbon price due to the increased processing of feed $CaCO_3$. However, some units show a different trend due to nonlinearities present in the model. For example, the cost of the carbonator is highest in \$60/tonne carbon price scenario due to a higher CaO conversion at lower CaO recycle rates.

Figure 6a shows that the cost of limestone purchase and disposal makes up a large proportion of the process OPEX. These costs could potentially be reduced by recycling $CaCO_3$ exported from the DAC unit back into the process (recycling the $CaCO_3$ disposal stream back to stream 1 in ESI Figure 1b). However, since the carbon price is relatively high compared to the purchase + disposal cost (\$60/tonne - \$150/tonne vs \$8/tonne assumed in this work) this modification would result in a small difference in the process NPV, and would require further experimentation to determine how to incorporate the $CaCO_3$ particles produced in the DAC unit into the calcium loop. Recycling $CaCO_3$ from the DAC unit, however, may be required if there are limits on the amount of available feed $CaCO_3$ at a given location, e.g., the optimal design of the MiNG \$150 PJM scenario requires 10.6 Million metric tons per year of feed $CaCO_3$, which is around 10% of the North American limestone market volume in 2021 (1,159.10 Mt[44]).

### 3.3 Synergy of coupling flue gas $CO_2$ capture and DAC

To further explain the synergistic effect of coupling NGCC power production, flue gas $CO_2$ capture and direct air capture, two further case studies are analyzed and compared to the "coupled system" used in sections 3.1 and 3.2. The two other case studies are defined as follows:

1. "Decoupled system": In this case, the system is the same

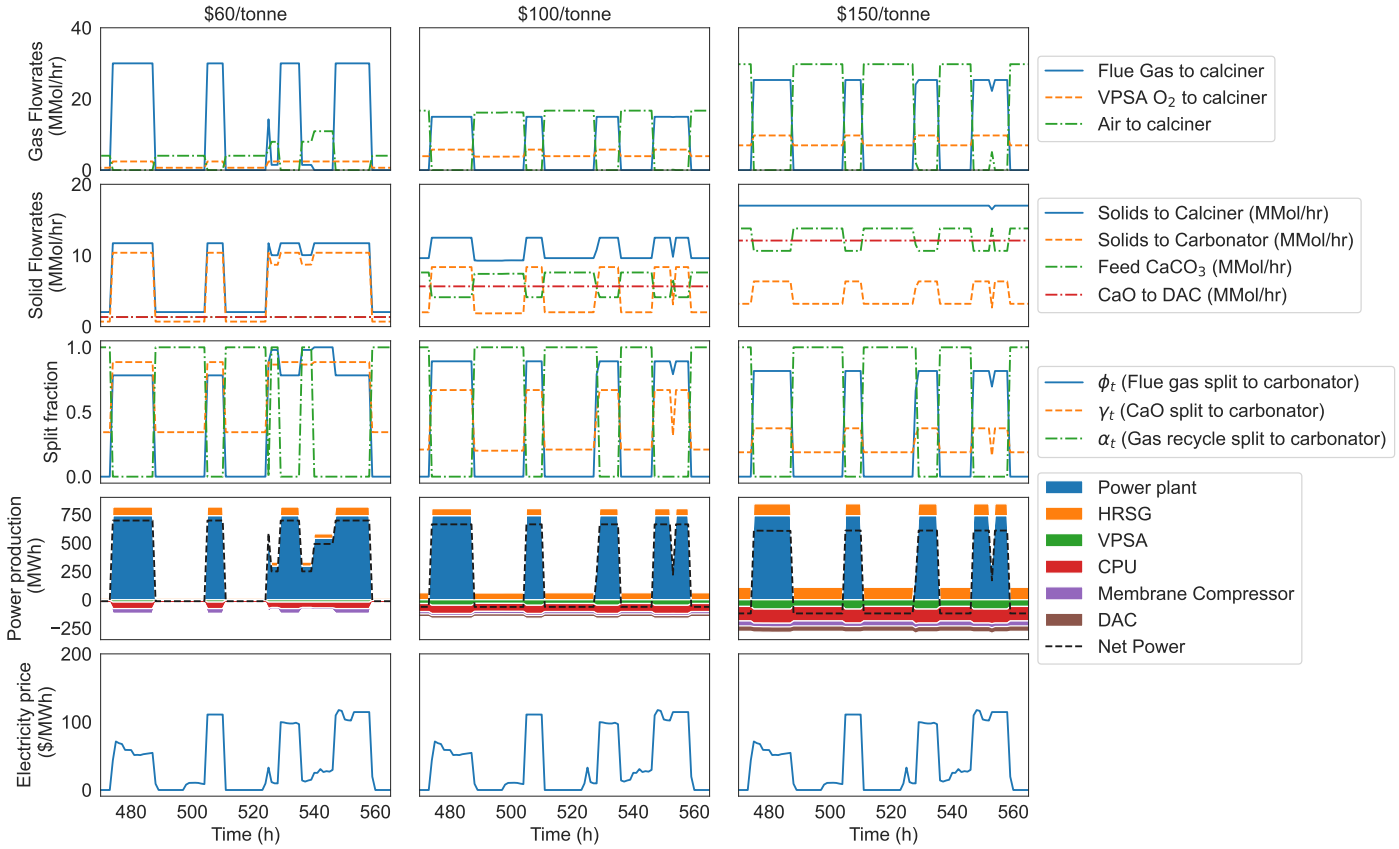


Fig. 5 Optimal dispatch for the MiNG $150 PJM market scenario with varying carbon prices. The label at the top of each column refers to the carbon price.

as before but NGCC flue gases (stream 7 in figure 1b) are vented to the atmosphere with an associated carbon tax. This case represents a co-located NGCC power plant facility and a Carbon 8 + DAC facility that are not thermally or mass integrated, but are electrically integrated. The Carbon 8 + DAC system does not need to react to large variations in the flue gas flowrate.

2. "Carbon8 + DAC system": In this case, the system is simply the Carbon 8 + DAC facility, that imports electricity from the grid to support operations. There is no NGCC.

Figure 7 highlights the optimal plant dispatch for the three systems over 4 representative days under the MiNG $150 PJM market scenario. The optimal operation of the decoupled system and the Carbon8 + DAC system is similar to that of the coupled system at time of low electricity prices when the NGCC is off, except the CaO flow rate to DAC is lower in the coupled system due to an increased average recycle rate of CaO to the carbonator †. In the decoupled system and Carbon8 + DAC system, all sections of the capture plant operate at a constant rate regardless of the electricity price, which, from an operational perspective, is advantageous over the coupled system. Note that in the decoupled system, it is still optimal to build a carbonator in cases where no flue gases enter the system, in which case the carbonator only operates to capture recycled $CO_2$ from the membrane and CPU units.

In Table 2 we show a comparison of the optimized results for the three case studies. When modeling the decoupled system, the Carbon8 + DAC system is not built at carbon prices of $60/tonne and $100/tonne, and therefore the NPV decreases by 56% (0.995 to 0.442 $ bn) between carbon prices of $60/tonne and $100/tonne, primarily due to the increased cost of venting $CO_2$ to the atmosphere. Similarly, the Carbon8 + DAC system is not deployed at carbon prices of $60/tonne and $100/tonne in the system without an NGCC plant. However, at a carbon prices of $150/tonne and above, the Carbon8 + DAC system is built in all cases (coupled system, decoupled system and Carbon8 + DAC system without NGCC). The NPV and process design outcomes for three process cases in Table 2 suggests that at carbon prices of $60/tonne and $100/tonne, it is optimal to operate the NGCC plant without $CO_2$ capture (decoupled system without Carbon8 + DAC deployment), where the near 50% capacity utilization of the power plant makes it more economical to incur the penalty of $CO_2$ emissions rather than investing the available $CO_2$ capture technology. In contrast, at carbon prices of $150/tonne, the coupled system yields the maximum NPV which is $137 M higher compared to the decoupled system ($1.966 bn vs $1.829 bn respectively) as well as $681 M higher than that of System without

† This is because when the NGCC is on, a portion of CaO is required for flue gas $CO_2$ capture in the carbonator for the coupled case.

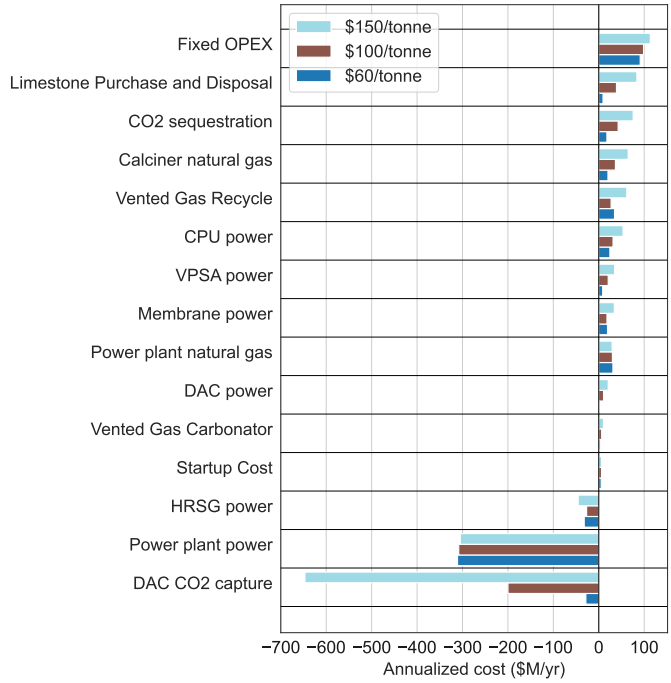


(a) Breakdown of OPEX for the MiNG $150 PJM market scenario with varying carbon prices. Negative values for annualised cost correspond to process revenues.

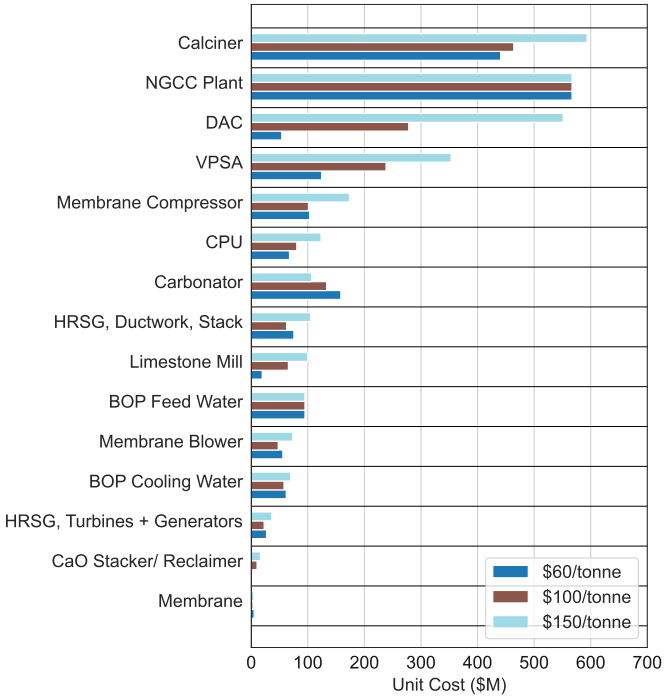


(b) Breakdown of CAPEX for the MiNG $150 PJM market scenario with varying carbon prices. The unit costs shown here include not only the base cost for the equipment, but also direct labor, bare erect cost, Engineering, Construction Management, Home Office & Fees (Eng'g CM, H.O. & Fees).

Fig. 6

NGCC. This quantifies the benefit of synergistic integration between the Carbon 8 + DAC system and the NGCC plant. It is also interesting to note that coupled system results in 3.7% greater utilization of the NGCC power and 1.8% greater net power exports in the $150/tonne scenarios as compared to the decoupled system, while at the same time producing greater negative emissions. This result is a direct consequence of mass and thermal integration between the NGCC power plant and the Carbon8 + DAC system, notably in the use of flue gas rather than air for $O_2$ supply for the calciner. When compared to the Carbon8 + DAC facility alone ("Carbon8 + DAC" in Table 2), the coupled system is able to reduce the average cost of energy requirement for DAC by avoiding power purchases during periods of high electricity prices.

The slightly lower NPV for the decoupled system compared to the coupled system in the $150/tonne carbon price scenario can be explained by a few competing effects, as shown in figures 8a and 8b. First, the decoupled system has a large carbon tax (160 $M/yr) for venting $CO_2$ to the atmosphere, but in the coupled system it is still economical to vent some of the recycled gases from the membrane and CPU separation systems, amounting to 60 $M/yr in tax for venting recycled gases. Second, the net amount of $CO_2$ captured by the DAC facility in the decoupled system is higher in the coupled system since less CaO is recycled to the carbonator and hence more CaO is available for DAC. However, due to the higher amount of vented $CO_2$, the decoupled system results in 3% smaller net negative $CO_2$ emissions than the coupled system in the $150/tonne case. Third, the capital expenditure for the carbonator is higher in the coupled system due to the increased solids requirement for flue gas $CO_2$ capture. Collectively, these factors explain the lower NPV for the decoupled system vs. the coupled system.

## 4 Conclusions

In this work we determined the optimal design and operation of a novel negative emissions power plant concept that couples flue gas $CO_2$ capture via calcium looping with lime-based DAC. The process is designed to respond flexibly to the highly volatile electricity price profiles expected in future variable renewable energy (VRE)- dominated electricity grids. At the same time, negative emissions are enabled in a synergistic manner. To evaluate such a concept, we propose a generalized design and operations framework that represents nonlinear physics and cost characterization of key unit operations as well as accounting for temporal variability in electricity prices in a computationally tractable manner. To determine the economic viability of the plant under different future market scenarios, net present value (NPV) maximizations were conducted under alternative market scenarios for electricity prices, carbon prices and natural gas prices.

The findings highlight the opportunity for the process to be deployed under carbon prices at or near $150/tonne, which is consistent with recent policy initiatives, such as the Inflation Reduction Act, to promote DAC technology deployment. Under market scenarios where the process is profitable, the optimal operation

Table 2 Optimized process NPVs and key metrics for the MiNg $150 PJM scenario with varying carbon prices. *$CO_2$ capture rate excluding DAC as a fraction of $CO_2$ input to the system (the total $CO_2$ that enters the system, including $CO_2$ present in calcium carbonate and natural gas). Coupled system refers to the integrated NGCC Carbon8 + DAC system with flue gas entering the calcium loop. Decoupled system refers to the NGCC Carbon8 + DAC system where flue gas is vented. Carbon8 + DAC refers to the standalone Carbon8 + DAC system without the NGCC plant. .

| **Case study →** | | **Coupled system** | | | | **Decoupled System** | | | | **Carbon8 + DAC** | | | |
|---|---|---|---|---|---|---|---|---|---|---|---|---|---|
| **Carbon Price** | **$/ton** | **60** | **100** | **150** | **200** | **60** | **100** | **150** | **200** | **60** | **100** | **150** | **200** |
| Carbon8 + DAC deployed? | | yes | yes | yes | yes | no | no | yes | yes | no | no | yes | yes |
| NPV | $bn | -0.600 | -0.200 | 1.966 | 4.314 | 0.995 | 0.442 | 1.829 | 4.129 | 0 | 0 | 1.285 | 4.209 |
| Fraction of hours NGCC on | - | 0.552 | 0.521 | 0.516 | 0.489 | 0.531 | 0.520 | 0.491 | 0.460 | 0 | 0 | 0 | 0 |
| NGCC power | TWh/yr | 3.472 | 3.362 | 3.286 | 3.053 | 3.419 | 3.363 | 3.167 | 2.977 | 0 | 0 | 0 | 0 |
| Net power | TWh/yr | 3.214 | 2.764 | 2.205 | 1.967 | 3.419 | 3.363 | 2.166 | 1.952 | 0 | 0 | -1.001 | -1.025 |
| $CO_2$ capture efficiency* | - | 0.740 | 0.927 | 0.940 | 0.945 | - | - | 0.994 | 0.992 | - | - | 0.994 | 0.992 |
| Net $CO_2$ emissions | ton/yr | 0.155 | -1.663 | -3.832 | -3.918 | 1.159 | 1.139 | -3.727 | -3.830 | 0 | 0 | -4.801 | -4.838 |
| Upper Bound | $bn | -0.593 | -0.200 | 1.97 | 4.378 | 0.995 | 0.442 | 1.858 | 4.169 | 0 | 0 | 1.313 | 4.250 |
| Abs. Gap | $bn | 0.007 | 0 | 0.004 | 0.064 | 0 | 0 | 0.029 | 0.041 | 0 | 0 | 0.029 | 0.041 |
| Rel. Gap | (%) | 1.186 | 0 | 0.186 | 1.495 | 0 | 0 | 1.579 | 0.99 | - | - | 2.243 | 0.971 |

offers several advantages as compared to traditional schemes for natural gas power generation with carbon capture: 1) Power is exported from the plant at high electricity prices and imported at low electricity prices, thus leveraging the variability in the electricity price to maximize profit. 2) Under market scenarios where the project is profitable, all process units (with the exception of the NGCC power plant and the vacuum pressure swing adsorption unit) run continuously with high capex utilization over yearly operation. The optimization results highlight the optimal time trajectories of some key process variables, the optimal sizing/ capital expenditure for each process unit, and some key economic/ sustainability metrics over yearly operation of the plant. These optimization results may be used to guide further design configurations and experiments.

The synergistic integration between the Carbon8 + DAC system and the NGCC plant is quantified by the observation of higher NPVs, higher negative emissions and higher power exports compared to involving co-located DAC and power plant where the flue gas is not captured via the calcium looping system. In addition, the integrated concept results in 52% greater NPV than standalone Carbon8+DAC system producing only negative emissions by reducing the cost of energy input for DAC during periods of high grid electricity prices.

While we have conducted NPV maximizations for a particular FLECCS process, the general approach to global optimization outlined in this work may be used as a template to analyze other processes where the optimal design and operational schedule may vary significantly with respect to a time-varying electricity prices. The process optimization shown here may be readily extended to consider different design considerations for the proposed FLECCS process. In particular, the impact of ambient temperature on the kinetics of batch based DAC process are not considered in this work. Thus, further amendments to the optimization may be required to consider ambient effects based on time and location. For this integrated FLECCS system to keep operating, rather than heating the air contactor the generated calcium oxide can be stored during cold temperatures for later discharge. The current model already includes a stacker, reclaimer, and storage unit. Thus, the storage unit may need to be upscaled depending on the location's climate.

## Author Contributions

Edward J. Graham: Conceptualization, data curation, formal analysis, investigation, methodology, Software, Validation, Visualization, writing – original draft, writing – review & editing. Moataz Sheha: Data curation, writing – review & editing, Software. Dharik Mallapragada: Conceptualization, Supervision, Funding acquisition, Methodology, Writing – review & editing. Howard Herzog: Project administration, Supervision, Funding acquisition, Writing – review & editing. Emre Gençer: Supervision, Funding acquisition, Writing – review & editing. Phillip Cross: Data curation, Supervision, Funding acquisition, Writing – review & editing. James Custer: Data curation, Funding acquisition, Writing – review & editing. Adam Goff: Data curation, Funding acquisition, Writing – review & editing. Ian Cormier: Data curation, Funding acquisition, Writing – review & editing.

## Conflicts of interest

8 Rivers is the inventor and developer of Carbon8 and Calcite Direct Air Capture Technologies.

## Acknowledgements

This research was funded by Advanced Research Projects Agency–Energy (ARPA-E). Grant Number DE-AR0001311.

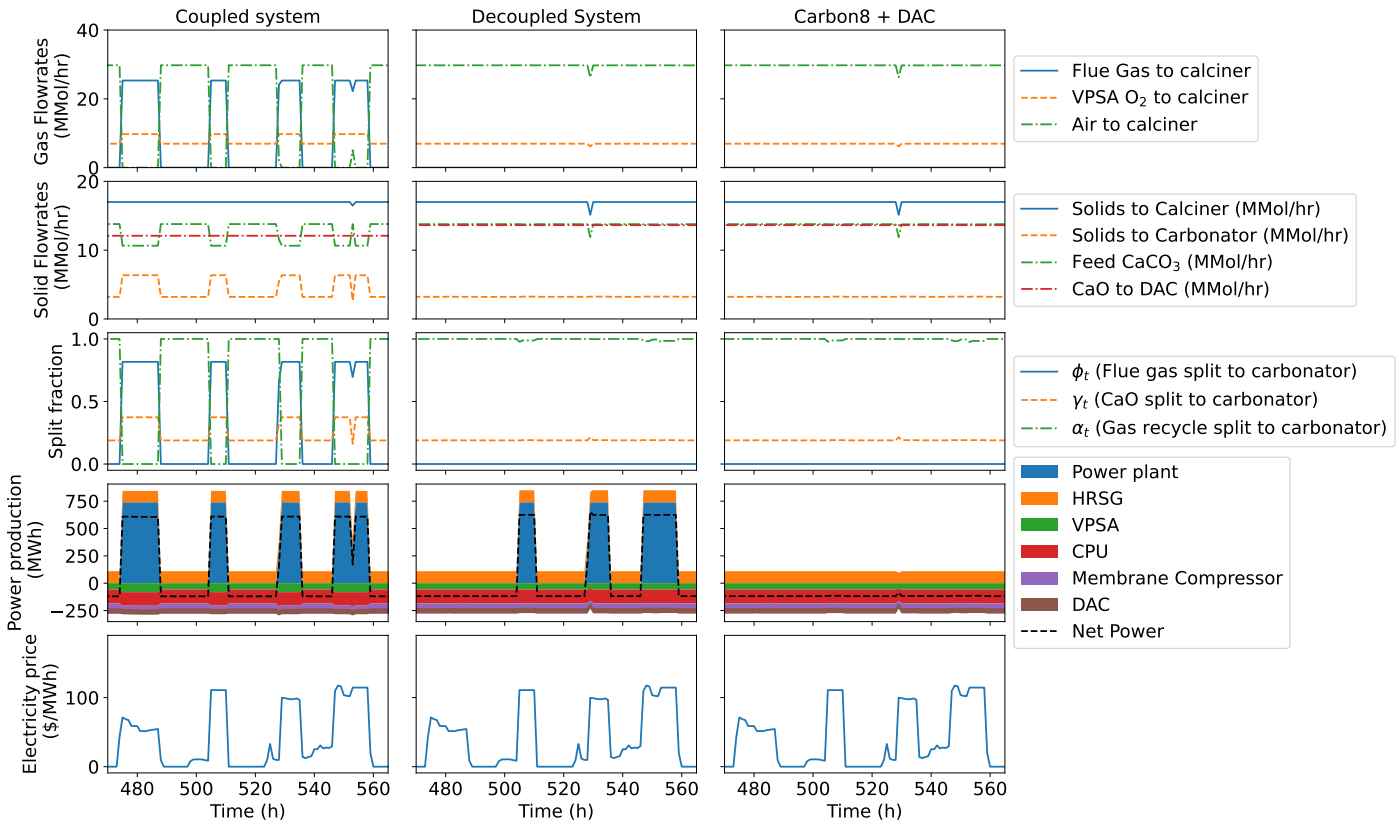


Fig. 7 Optimal dispatch for the MiNG $150 PJM market scenario.

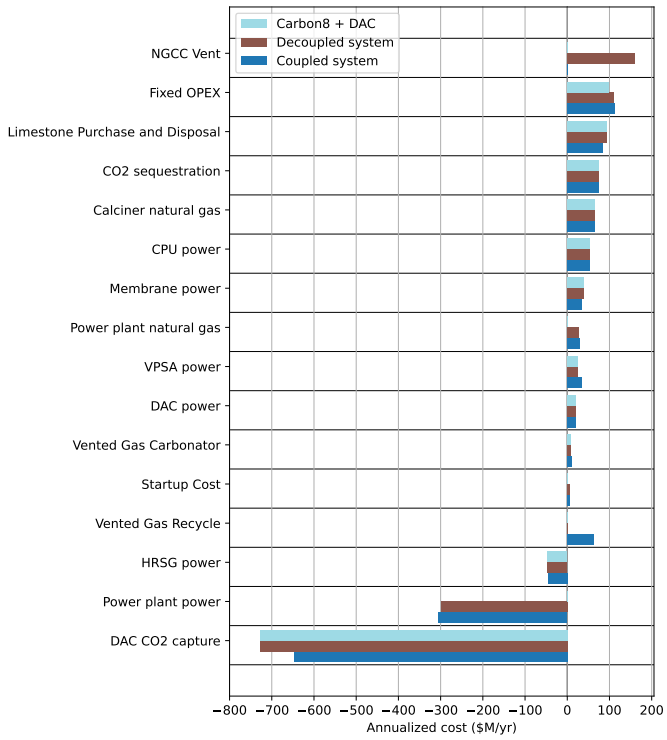


(a) Breakdown of OPEX for the MiNG $150 PJM market scenario with varying carbon prices.

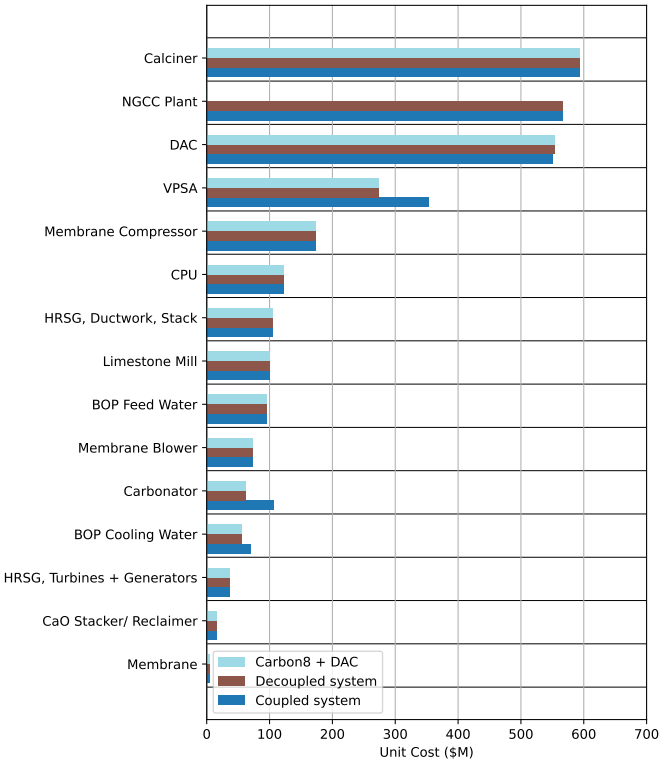


(b) Breakdown of CAPEX for the MiNG $150 PJM market scenario with varying carbon prices. The unit costs shown here include not only the base cost for the equipment, but also direct labor, bare erect cost, Eng'g CM, H.O. fees and project contingencies.

Fig. 8

## References


1 S. J. Davis, N. S. Lewis, M. Shaner, S. Aggarwal, D. Arent, I. L. Azevedo, S. M. Benson, T. Bradley, J. Brouwer, Y.-M. Chiang, C. T. M. Clack, A. Cohen, S. Doig, J. Edmonds, P. Fennell, C. B. Field, B. Hannegan, B.-M. Hodge, M. I. Hoffert, E. Ingersoll, P. Jaramillo, K. S. Lackner, K. J. Mach, M. Mastrandrea, J. Ogden, P. F. Peterson, D. L. Sanchez, D. Sperling, J. Stagner, J. E. Trancik, C.-J. Yang and K. Caldeira, *Science*, 2018, **360**,.

2 J. E. Bistline, *Joule*, 2021, **5**, 2551–2563.

3 A. Mileva, J. Johnston, J. H. Nelson and D. M. Kammen, *Applied Energy*, 2016, **162**, 1001–1009.

4 N. A. Sepulveda, J. D. Jenkins, F. J. de Sisternes and R. K. Lester, *Joule*, 2018, **2**, 2403–2420.

5 H. Daggash, C. Heuberger and N. M. Dowell, *International Journal of Greenhouse Gas Control*, 2019, **81**, 181–198.

6 P. J. Heptonstall and R. J. K. Gross, *Nature Energy*, 2020, **6**, 72–83.

7 K. Z. House, C. F. Harvey, M. J. Aziz and D. P. Schrag, *Energy & Environmental Science*, 2009, **2**, 193.

8 S. Vasudevan, S. Farooq, I. A. Karimi, M. Saeys, M. C. Quah and R. Agrawal, *Energy*, 2016, **103**, 709–714.

9 G. G. Esquivel-Patiño, M. Serna-González and F. Nápoles-Rivera, *Energy Conversion and Management*, 2017, **151**, 334–342.

10 R. Domenichini, L. Mancuso, N. Ferrari and J. Davison, *Energy Procedia*, 2013, **37**, 2727–2737.

11 N. M. Dowell and N. Shah, *Energy Procedia*, 2014, **63**, 1525–1535.

12 D. L. Oates, P. Versteeg, E. Hittinger and P. Jaramillo, *International Journal of Greenhouse Gas Control*, 2014, **27**, 279–288.

13 M. S. Zantye, A. Arora and M. F. Hasan, *Computers & Chemical Engineering*, 2019, **130**, 106544.

14 M. S. Zantye, A. Arora and M. M. F. Hasan, *Energy & Environmental Science*, 2021, **14**, 3986–4008.

15 F.-C. Yu, N. Phalak, Z. Sun and L.-S. Fan, *Industrial & Engineering Chemistry Research*, 2011, **51**, 2133–2142.

16 C. Dean, J. Blamey, N. Florin, M. Al-Jeboori and P. Fennell, *Chemical Engineering Research and Design*, 2011, **89**, 836–855.

17 N. Rodríguez, R. Murillo and J. C. Abanades, *Environmental science & technology*, 2012, **46**, 2460–2466.

18 E. D. Lena, M. Spinelli, M. Gatti, R. Scaccabarozzi, S. Campanari, S. Consonni, G. Cinti and M. C. Romano, *International Journal of Greenhouse Gas Control*, 2019, **82**, 244–260.

19 E. Robert, D. Kearins, M. Turner, M. Woods, N. Kuehn and A. Zoelle, *Cost and performance baseline for fossil energy plants volume 1: bituminous coal and natural gas to electricity*, National energy technology laboratory (netl), pittsburgh, pa, morgantown, wv ... technical report, 2019.

20 E. S. Rubin and H. Zhai, *Environmental science & technology*, 2012, **46**, 3076–3084.

21 E. Mechleri, P. S. Fennell and N. M. Dowell, *International Journal of Greenhouse Gas Control*, 2017, **59**, 24–39.

22 S. M. Cohen, G. T. Rochelle and M. E. Webber, *International Journal of Greenhouse Gas Control*, 2012, **8**, 180–195.

23 M. Yuan, H. Teichgraeber, J. Wilcox and A. R. Brandt, *International Journal of Greenhouse Gas Control*, 2019, **84**, 154–163.

24 X. Peng, T. W. Root and C. T. Maravelias, *AIChE Journal*, 2018, **65**, e16458.

25 Q. Zhang, M. Martín and I. E. Grossmann, *Computers & Chemical Engineering*, 2019, **122**, 80–92.

26 D. S. Mallapragada, E. Gençer, P. Insinger, D. W. Keith and F. M. O'Sullivan, *Cell Reports Physical Science*, 2020, **1**, 100174.

27 N. M. Dowell and N. Shah, *Computers & Chemical Engineering*, 2015, **74**, 169–183.

28 S. Cohen and V. Durvasulu, *NREL Price Series Developed for the ARPA-E FLECCS Program*, 2021, `https://www.osti.gov/servlets/purl/1838046/`.

29 S. C. Jesse D Jenkins, *Summary Report of the GenX and PowerGenome runs for generating Price Series (for ARPA-E FLECCS Project)*, 2021, `https://zenodo.org/record/5765798`.

30 *FLExible Carbon Capture and Storage (FLECCS)*, https://arpa-e.energy.gov/technologies/programs/fleccs, Accessed: 2022-11-23.

31 M. Sheha, E. Graham, D. Mallapragada, E. Gencer, P. Cross, J. Custer, A. Goff, I. Cormier and H. Herzog, *engrXiv preprint*, 2023, DOI: 10.31224/3006.

32 A. Cozad, N. V. Sahinidis and D. C. Miller, *AIChE Journal*, 2014, **60**, 2211–2227.

33 P. S. Fennell, R. Pacciani, J. S. Dennis, J. F. Davidson and A. N. Hayhurst, *Energy & Fuels*, 2007, **21**, 2072–2081.

34 D. S. Mallapragada, D. J. Papageorgiou, A. Venkatesh, C. L. Lara and I. E. Grossmann, *Energy*, 2018, **163**, 1231–1244.

35 M. L. Bynum, G. A. Hackebeil, W. E. Hart, C. D. Laird, B. L. Nicholson, J. D. Siirola, J.-P. Watson and D. L. Woodruff, *Pyomo–optimization modeling in python*, Springer Science & Business Media, 3rd edn, 2021, vol. 67.

36 W. E. Hart, J.-P. Watson and D. L. Woodruff, *Mathematical Programming Computation*, 2011, **3**, 219–260.

37 Gurobi Optimization, LLC, *Gurobi Optimizer Reference Manual*, 2022, `https://www.gurobi.com`.

38 A. Reuther, J. Kepner, C. Byun, S. Samsi, W. Arcand, D. Bestor, B. Bergeron, V. Gadepally, M. Houle, M. Hubbell, M. Jones, A. Klein, L. Milechin, J. Mullen, A. Prout, A. Rosa, C. Yee and P. Michaleas, 2018 IEEE High Performance extreme Computing Conference (HPEC), 2018, pp. 1–6.

39 *Carbon Capture Provisions in the Inflation Reduction Act of 2022*, https://cdn.catf.us/wp-content/uploads/2022/08/19102026/carbon-capture-provisions-ira.pdf, Accessed: 2022-11-23.

40 D. W. Keith, G. Holmes, D. S. Angelo and K. Heidel, *Joule*, 2018, **2**, 1573–1594.

41 X. Zhang and Y. Liu, *Applied Thermal Engineering*, 2014, **70**, 13–24.

42 S. M. Cohen, G. T. Rochelle and M. E. Webber, *Energy Procedia*, 2011, **4**, 2604–2611.

43 A.-M. Cormos and A. Simon, *Applied Thermal Engineering*,

2015, **80**, 319–327.

44 *North America Limestone Market: Industry Trends, Share, Size, Growth, Opportunity and Forecast 2022-2027*, https://www.imarcgroup.com/north-america-limestone-market, Accessed: 2022-9-12.

# Optimization of a combined power plant $CO_2$ capture and direct air capture concept for flexible power plant operation

Electronic supplementary information (ESI)

Edward J. Graham[1], Moataz Sheha[1], Dharik S. Mallapragada[1], Howard J. Herzog[1], Emre Gençer[1], Phillip Cross[2], James Custer[2], Adam Goff[2], and Ian Cormier[2]

[1]MIT Energy Initiative, Massachusetts Institute of Technology, Cambridge, MA, USA.
[2]8 Rivers Capital, Durham, USA

Electronic supplementary information for the paper 'Optimization of a flexible carbon capture process coupled with direct air capture'. Section S1 describes the process model equations and fixed parameters used in the optimizations. Section S2 describes the equations used in the net present value calculation. Section S3 describes the method used to develop an analytical equation for the CaO conversion in the carbonator. Section S4 describes the k-means clustering algorithm that is used to reduce the time-dimensionality of the optimization model. Section S5 describes the methodology for developing a surrogate model for the membrane unit. Finally, two other case studies are presented to support the dissusions in the main text, a case where the carbon price is raised to $200/tonne (Section S6), and another case where all gases are recycled from the separation units to the carbonator (Section S7).

## S1 Process Model

A schematic of the process model is shown in the main text (Figure 1). Variables used in this section are defined in Table S1. Model parameters are defined in Tables S2 and S4.

**Table S1** List of variables used within the optimization model.

| Variable | Description | Units |
|---|---|---|
| *Process variables* | | |
| $F_t^{NG,PP}$ | Natural gas flowrate to NGCC plant | MMol $^{-1}$ |
| $F_{i,j,t}^{s}$ | Molar flowrate of stream $i$ and component $j$ at time $t$ | MMol hr$^{-1}$ |
| $F_{i,t}^{s,tot}$ | Total molar flowrate of stream $i$ | MMol hr$^{-1}$ |
| $z_{i,j,t}^{s}$ | Mole fraction of stream $i$ and component $j$ at time $t$ | - |
| $F_{i,j,t}^{gl}$ | Molar flowrate of stream $i$ and component $j$ at time $t$ | MMol hr$^{-1}$ |
| $F_{i,t}^{gl,tot}$ | Total molar flowrate of stream $i$ | MMol hr$^{-1}$ |
| $z_{i,j,t}^{gl}$ | Mole fraction of stream $i$ and component $j$ at time $t$ | - |
| $F_{i,j,t}^{b}$ | Molar flowrate of stream $i$ and component $j$ at time $t$ | MMol hr$^{-1}$ |
| $F_{i,t}^{b,tot}$ | Total molar flowrate of stream $i$ | MMol hr$^{-1}$ |
| $z_{i,j,t}^{b}$ | Mole fraction of stream $i$ and component $j$ at time $t$ | - |
| $y_{f,CO_2,t}$ | Mole fraction of $CO_2$ in membrane feed | |
| $y_{p,CO_2,t}$ | Mole fraction of $CO_2$ in membrane permeate | |
| $y_{r,CO_2,t}$ | Mole fraction of $CO_2$ in membrane retentate | |
| $W_t$ | Power | GW |
| $Q_t^u$ | Heat input to unit $u$ | GW |
| $\zeta_t$ | Extent of reaction | MMol hr$^{-1}$ |
| $\gamma_t$ | Fraction of stream 3 split to carbonator | - |
| $\phi_t$ | Fraction of stream 7 split to carbonator | - |
| $\alpha_t$ | Fraction of stream 22 split to carbonator | - |
| $P_t$ | Pressure of stream 17 entering the membrane | bar |
| $\bar{X}_t^{carb}$ | Average $CaO$ conversion in the carbonator | - |
| $nCaODAC_t$ | Storage inventory before DAC | MMol |
| $CaO_{use}$ | CaO flowrate from storage to DAC | MMol hr$^{-1}$ |
| $y_t$ | Binary variable denoting on/off state of the NGCC plant (1 is on, 0 is off) | - |
| $s_t$ | Binary variable to track whether the NGCC turns on between consecutive time steps | - |
| $A$ | Membrane area | Mm$^2$ |

**Table S1 – continued from previous page**

| Variable | Description | Units |
|---|---|---|
| $\bar{\sigma}$ | Dimensionless membrane area divided by retentate pressure (see S5) | $bar^{-1}$ |
| $\Delta H_t$ | Enthalpy change between carbonator off-gas (stream 10) and the vented stream after providing heat to the dryer and HRSGG | GW |
| $Q_t^{dryer}$ | Heat requirement for the dryer | GW |
| $Cduty_t^{PP}$ | Power plant coolind duty | GW |
| $Cduty_t^{Carbon8}$ | Cooling duty for Carbon8 system | GW |
| $W_t^{PP}$ | Electricity production from power plant | GW |
| $W_t^{HRSG}$ | Electricity production from HRSG | GW |
| $W_t^{VPSA}$ | Electricity requirement for VPSA | GW |
| $W_t^{CPU}$ | Electricity requirement for CPU | GW |
| $W_t^{DAC}$ | Electricity requirement for DAC | GW |
| $W_t^{Compressor}$ | Electricity requirement for compression before membreane | GW |
| *Capacity/ costing variables* | | |
| $capFlow_{calciner}$ | Maximum flow rate of calciner solids input (stream 2) | Mmol/hr |
| $capFlow_{carbonator}$ | Maximum flow rate of carbonator solids input (stream 5) | Mmol/hr |
| $capFlow_{LimestoneMill}$ | Maximum flow rate of solids exiting the limestone mill (stream 1) | Mmol/hr |
| $capFlow_{Blower}$ | Maximum flowrate of gases entering the blower (stream 16) | Mmol/hr |
| $capFlow_{VPSA}$ | Maximum flowrate of gases exiting the VPSA (stream 11) | Mmol/hr |
| $capFlow_{HRSG,turbines+generators}$ | Maximum power produced by the HRSG | GW |
| $capFlow_{HRSG,ductwork+stack}$ | Maximum power produced by the HRSG | GW |
| $capFlow_{MembraneCompressor}$ | Maximum compression work before membrane | GW |
| $capFlow_{BOPCoolingWater}$ | Maximum cooling water duty | GW |
| $cap_{DACstorage}$ | Maximum storage inventory in DAC storage unit | Mmol |
| $flowRatio_u$ | Ratio of capacity flow and base case flow ($bcf_u$) | - |
| $unitCost_u$ | Cost for unit $u$ | $M |
| $c_{membrane}$ | Cost of membrane per unit area | $M/Mm$^2$ |
| $CAPEX_{annualized}$ | Annualized total capital cost of the plant | $M |
| $opex_t^{CPU}$ | Electricity cost for CPU | $M/hr |
| $opex_t^{Membrane}$ | Electricity cost for membrane compression | $M/hr |
| $opex_t^{DAC}$ | Electricity cost for DAC | $M/hr |
| $opex_t^{PowerPlantNG}$ | Cost of natural gas to NGCC plant | $M/hr |
| $opex_t^{CalcinerNG}$ | Cost of natural gas to Calciner | $M/hr |
| $opex_t^{VPSA}$ | Electricity cost for VPSA | $M/hr |
| $opex_t^{LimestonePurchase}$ | Cost of limestone purchase | $M/hr |
| $opex_t^{LimestoneDisposal}$ | Cost of limestone disposal | $M/hr |
| $opex_t^{VentedGasRecycle}$ | Carbon cost of venting recycled gases | $M/hr |
| $opex_t^{VentedGasCarbonator}$ | Cost of venting off-gases from carbonator | $M/hr |
| $opex_t^{CO_2Sequestration}$ | Cost of $CO_2$ sequestration | $M/hr |
| $opex_t^{Startup}$ | Cost of starting up the NGCC plant | $M/hr |
| $OPEX_{var,annual}$ | Total variable annual OPEX | $M/yr |
| $OPEX_{fixed,annual}$ | Total fixed annual OPEX | $M/yr |
| $OPEX_{annual}$ | Total annual OPEX | $M/yr |
| $revenue_t^{PowerPlant}$ | Revenues from NGCC electricity generation | $M/hr |
| $revenue_t^{HRSG}$ | Revenues from HRSG electricity generation | $M/hr |
| $revenue_t^{DAC}$ | Revenues from DAC $CO_2$ removal | $M/hr |
| $REVENUE_{annual}$ | Total annual revenue | $M/yr |
| $NPV$ | Net present value of project | $M |
| *Subscripts* | | |
| $i$ | Stream | |
| $j$ | Component | |
| $t$ | Time | hr |
| *Superscripts* | | |
| $tot$ | Total flow rate | |
| $PP$ | Power Plant | |
| $carb$ | Carbonation reaction | |
| $calc$ | Calcination reaction | |
| $comb$ | Combustion reaction | |
| $CAP$ | Maximum Capacity | |

**Table S1 – continued from previous page**

| Variable | Description | Units |
|---|---|---|
| $gl$ | Gas or liquid streams | |
| $s$ | Solid streams | |
| $b$ | Binary mixture of $CO_2$ and $N_2$ | |

**Table S2** List of Parameters used within the optimization model.

| Parameter | Description | Value | Units |
|---|---|---|---|
| $N_t$ | Number of hours | 720 | hr |
| $X^{CaO,DAC}$ | DAC conversion | 0.9 | - |
| $X^{calc}$ | Conversion of $CaCO_3$ in the calciner | 1 | - |
| $X^{carb,CO_2}$ | $CO_2$ conversion in the carbonator | 0.95 | - |
| *Flow rates/ compositions* | | | |
| $F^{s}_{1,CaO,t}$ | Feed CaO | 0 | MMol/hr |
| $z^{gl}_{7,CO_2,t}$ | Mole fraction of flue gas | 0.044 | - |
| $z^{gl}_{7,O_2,t}$ | Mole fraction of flue gas | 0.113 | - |
| $z^{gl}_{7,H_2O,t}$ | Mole fraction of flue gas | 0.093 | - |
| $z^{gl}_{7,N_2,t}$ | Mole fraction of flue gas | 0.075 | - |
| $z^{gl}_{7,CH4,t}$ | Mole fraction of flue gas | 0.093 | - |
| $z^{gl}_{12,CO_2,t}$ | Mole fraction of VPSA outlet | 0 | - |
| $z^{gl}_{12,O_2,t}$ | Mole fraction of VPSA outlet | 0.95 | - |
| $z^{gl}_{12,H_2O,t}$ | Mole fraction of VPSA outlet | 0 | - |
| $z^{gl}_{12,N_2,t}$ | Mole fraction of VPSA outlet | 0.05 | - |
| $z^{gl}_{12,CH4,t}$ | Mole fraction of VPSA outlet | 0 | - |
| $z^{gl}_{13,CO_2,t}$ | Mole fraction of natural gas to calciner | 0 | - |
| $z^{gl}_{13,O_2,t}$ | Mole fraction of natural gas to calciner | 0 | - |
| $z^{gl}_{13,H_2O,t}$ | Mole fraction of natural gas to calciner | 0 | - |
| $z^{gl}_{13,N_2,t}$ | Mole fraction of natural gas to calciner | 0 | - |
| $z^{gl}_{13,CH4,t}$ | Mole fraction of natural gas to calciner | 1 | - |
| $c^{21}_{CO_2}$ | Purity constraint for $CO_2$ sequestration | 0.95 | - |
| *Regression coefficients* | | | |
| $c^{b}_{19,CO_2}$ | Linear coefficient for inlet $CO_2$ flowrate to distillation | 1.2851 | - |
| $c^{tot,b}_{19,CO_2}$ | Linear coefficient for total (permeate) flowrate to distillation | -0.2425 | - |
| $c^{PP}_{1}$ | Coefficient for relating NGCC power to Flue gas flowrate | 5.845 | MMol/GWh |
| $c^{PP}_{2}$ | Coefficient for relating NGCC power to Flue gas flowrate | 1.0543 | MMol/h |
| $c^{PP,CAP,min}$ | Minimum stable operation of NGCC plant as a fraction of full capacity | 0.4 | - |
| $c^{NG,PP}$ | Coefficient relating NGCC flue gas flowrate to natural gas flowrate | 25.7 | - |
| $c^{tot,gl}_{11}$ | - | 11.098 | - |
| $c^{tot,gl}_{8}$ | - | 0.7411 | - |
| $c^{tot,gl}_{12}$ | - | 2.036 | - |
| $c^{tot,s}_{1}$ | - | 8.652 | - |
| $c^{tot,s}_{6,CaCO_3}$ | - | 7.403 | - |
| $c^{tot,s}_{6,CaO}$ | - | 1 | - |
| $c^{quench}$ | Coefficient used to determine the amount of water used in quenching | 0.0457 | - |
| $c^{waterremoval}$ | Fraction of water removed by flash, compressor knockout and dryer | 0.012 | - |
| $c^{Qdryer}$ | Thermal energy coefficient for dryer | 0.0245 | GW/MMol |
| $c^{lnP}_{1}$ | Linear coefficient for ln $P_t$ | 0.1933 | - |

**Table S2 – continued from previous page**

| Parameter | Description | | Units |
|---|---|---|---|
| $c_2^{lnP}$ | Linear coefficient for ln $P_t$ | 0.5888 | - |
| $c^{Cduty,PP}$ | Coefficient defining the relationship between power plant cooling duty and flow rate of NGCC flue gas (stream 7) | 0.00295 | GW/(Mmol/hr) |
| $c^{Cduty,Carbon8}$ | Coefficient defining the relationship between Carbon8 cooling duty and flow rate of calciner off-gas (stream 14) | 0.0138 | GW/(Mmol/hr) |
| $c^{comp}$ | Coefficient for compressor power scaling | 1.138 | - |
| $c^{WVPSA}$ | Relation between VPSA power requirement and flow rate of stream 11 | 0.00842 | GW/(Mmol/hr) |
| $c^{WCPU}$ | Relation between CPU power requirement and permeate flowrate (stream 19) | 0.492 | GW/(Mmol/hr) |
| $c^{WDAC}$ | Relation between DAC power requirement and CaO flowrate to DAC | 0.00842 | GW/(Mmol/hr) |
| *Membrane surrogate model coefficients* | | | |
| $c_1^{surr}$ | | -0.0118 | bar |
| $c_2^{surr}$ | | 0.000119 | $bar^2$ |
| $c_3^{surr}$ | | 0.311 | - |
| $c_4^{surr}$ | | -0.00559 | bar |
| $c_5^{surr}$ | | 0.0308 | $bar^-1$ |
| $c_6^{surr}$ | | 2.643 | - |
| $c_7^{surr}$ | | -2.394 | - |
| *Experimental coefficients* | | | |
| $Perm_{CO_2}$ | $CO_2$ permeance in the membrane | 0.000484 | MMol/hr/$m^2$/bar |
| $Perm_{N_2}$ | $N_2$ permeance in the membrane | 0.00002 | MMol/hr/$m^2$/bar |
| $f_m$ | How fast the CaO carrying capacity approaches $f_w$ | 0.7 [1] | - |
| $f_w$ | Carrying capacity of CaO when the number of cycles approaches infinity | 0.25 [1] | - |
| $h_{9,H_2O}$ | Pure component enthalpy of flue gas stream to carbonator | -239.94 | GJ/MMol |
| $h_{9,CO_2}$ | Pure component enthalpy of flue gas stream to carbonator | -391.3 | GJ/MMol |
| $h_{9,O_2}$ | Pure component enthalpy of flue gas stream to carbonator | 1.71 | GJ/MMol |
| $h_{9,N_2}$ | Pure component enthalpy of flue gas stream to carbonator | 1.69 | GJ/MMol |
| $h_{23,CO_2}$ | Pure component enthalpy of gas recycle stream | -394.1 | GJ/MMol |
| $h_{23,N_2}$ | Pure component enthalpy of gas recycle stream | 0.396 | GJ/MMol |
| $h_{5,CaCO_3}$ | Pure component enthalpy of carbonator inlet solids | -1147.8 | GJ/MMol |
| $h_{5,CaO}$ | Pure component enthalpy of carbonator inlet solids | -605.7 | GJ/MMol |
| $h_{6,CaCO_3}$ | Pure component enthalpy of carbonator outlet solids | 1170.3 | GJ/MMol |
| $h_{6,CaO}$ | Pure component enthalpy of carbonator outlet solids | 616.2 | GJ/MMol |
| $h_{10,H_2O}$ | Pure component enthalpy of vented gas after HRSG | -233.76 | GJ/MMol |
| $h_{10,CO_2}$ | Pure component enthalpy of vented gas after HRSG | -383.67 | GJ/MMol |
| $h_{10,O_2}$ | Pure component enthalpy of vented gas after HRSG | 7.11 | GJ/MMol |
| $h_{10,N_2}$ | Pure component enthalpy of vented gas after HRSG | 6.89 | GJ/MMol |
| $c^{\eta^{HRSG}}$ | Relation between HRSG power and cooling duty | 0.384 | - |

**Table S2 – continued from previous page**

| Parameter | Description | | Units |
|---|---|---|---|
| $\bar{C}_p$ | Average heat capacity of calciner off-gas before and after HRSG | 0.0378 | GJ/MMol/K |
| $R$ | Ideal Gas Constant | 0.008314 | GJ/MMol.K |
| *Design specifications* | | | |
| $Q^{carb,loss}$ | Fixed carbonator heat loss | 10 | MW |
| $c^{T_{15}}$ | Temperature of stream 15 | 620 | C |
| $c^{T_{16}}$ | Temperature of stream 16 after HRSG | 180 | C |
| $c^{P_0}$ | Compression inlet pressure | 1 | bar |
| $capFlow^{max}_{Calciner}$ | Maximum flowrate of solids entering calciner (stream 2) | | Mmol/hr |
| $c^{excess_{O_2}}$ | Fraction of excess $O_2$ required for methane combustion | 0.03 | - |
| $z^{max,calciner}_{O_2}$ | Maximum mole fraction of $O_2$ to calciner in gas phase | 0.3 | - |
| $W^{PP,CAP}$ | NGCC power production capacity | 0.74 | GW |
| *Costing parameters* | | | |
| $c^{LimestonePurchase}$ | Cost of feed limestone, based on \$5/tonne | 0.0005 | \$M/Mmol |
| $c^{LimestoneDisposal}$ | Cost of limestone disposal, based on \$3/tonne | 0.0003 | \$M/Mmol |
| $c^{Sequestration}$ | Cost of $CO_2$ sequestration, based on \$10/tonne | 0.00044 | \$M/Mmol |
| $EP_t$ | Electricity price | varies based on market scenario | \$M/GW |
| $FuelPrice$ | Fuel Price, based on 0.0224 MMBtu/lb HHV | varies based on market scenario | \$M/Mmol |
| $CarbonPrice$ | Carbon Price | varies based on market scenario | \$M/Mmol |
| $c^{StartUp}$ | Start up cost, based on 44\$/MW-cap (warm start) | $0.055W^{PP,CAP}$ | \$M/GW$^2$ |
| $c^{FixedOPEX}_1$ | Fixed OPEX parameter | 51.4 | \$M/yr |
| $c^{FixedOPEX}_2$ | Fixed OPEX parameter | 0.02 | \$M/yr/(\$M-CAPEX) |
| $CRF$ | Capital Recovery Factor, based on 30 years lifetime, 7.25% discount rate | 0.083 | - |
| $bcf_u$ | Flow rate used in the base case in the work of[3] | see table S4 | (varies) |
| $bf_u$ | Flow rate of unit with known cost | see table S4 | (varies) |
| $c_u$ | Cost of unit with known price | see table S4 | \$M |
| $e_u$ | Cost exponent | see table S4 | - |
| *Subscripts* | | | |
| $i$ | Stream | | - |
| $j$ | Component | | - |
| $t$ | Time | | hr |
| $u$ | Single or aggregated process unit | | - |
| *Superscripts* | | | |
| $PP$ | Power Plant | | |
| $CAP$ | Maximum Capacity | | |

## S1.1 Power plant model

Based on detailed Aspen Plus simulations of the NGCC plant[3], we found that it was reasonable to model the net power production as a linear function of the feed natural gas flow rate. The variation in flue gas composition with respect to net power is negligible for the purpose of this work. The power plant model is given by the following set of equations:

$$F^{NG,PP}_t = (c^{PP}_1 W^{PP}_t + c^{PP}_2) y_t \tag{S1}$$

$$W^{PP}_t \geq c^{PP,CAP,min} W^{PP,CAP} y_t \tag{S2}$$

$$W^{PP}_t \leq W^{PP,CAP} y_t \tag{S3}$$

$$F^{tot,gl}_{7,t} = c^{NG,PP} F^{NG,PP}_t \tag{S4}$$

$$s_t \geq y_t - y_{t-1} \quad t \in 2,...,N_t \tag{S5}$$

$$s_t \geq y_t - y_{N_t} \quad t = 1 \tag{S6}$$

Equation S1 relates the natural gas requirement to the NGCC power production. Coefficients $c_1^{PP}$ and $c_2^{PP}$ are determined via linear regression to the Aspen Plus model. $y_t$ is a binary variable denoting if the power plant is on ($y_t = 1$) or off ($y_t = 0$). In equation S2, a minimum stable loading operation with respect to the maximum capacity is enforced. Equation S3 ensures that no power is produced by the NGCC plant when it is off. Equation S4 relates the total flue gas flow rate to the natural gas flowrate, with $c^{NG,PP}$ determined from the Aspen Plus model. Equations S5 and S6 track start-up operation with a binary $s_t$ that equals 1 when the power plant switches from off to on between successive time points. Equations S5 and S6 determine the binary variable $s_t$ which tracks periods of start up of the NGCC plant and is used to calculate operational expenditures due to start-up. Here, Equation S6 defines the constraint for the first period by looking back at the state of the power plant at the last operational time step ($N_t$) of the year.

### S1.2 Solid streams

The following set of equations describe the mole balance on streams consisting only of solid components. Impurities that that may be part of the feed limestone such as other metal oxides are assumed to be negligible.

$$j_s = \{CaO, CaCO_3\} \tag{S7}$$
$$i_s = \{1,2,3,4,5,6\} \tag{S8}$$
$$F_{i_s,t}^{tot,s} = \sum_{j \in j_s} F_{i,j_s,t}^{s} \quad t \in \{1,...,N_t\} \tag{S9}$$
$$F_{2,j_s,t}^{s} = F_{1,j_s,t}^{s} + F_{6,j_s,t}^{s} \quad t \in \{1,...,N_t\} \tag{S10}$$
$$F_{3,j_s,t}^{s} = F_{4,j_s,t}^{s} + F_{5,j_s,t}^{s} \quad t \in \{1,...,N_t\}, \tag{S11}$$

Where stream 1 is the feed $CaCO_3$, stream 2 is the calciner inlet, stream 3 is the calciner outlet, stream 4 is the CaO stream sent to DAC, stream 5 is the CaO sent to the carbonator, and stream 6 is the carbonator solids outlet recycled to the calciner. The splitter after the calciner is modelled as

$$F_{5,j_s,t}^{s} = \gamma_t F_{3,j_s,t}^{s} \quad \gamma \in [0,1], \quad t \in \{1,...,N_t\} \tag{S12}$$

where $\gamma$ is the fraction of solids sent to the carbonator (the remainder 1-$\gamma$ is sent to the DAC unit). This introduces two bilinear terms to the optimization. While the addition of generalized reduction constraints can lead to a tighter relaxation of the non-convex formulation [4] (in this case, adding the redundant constraint $F_{4,j_s,t}^{s} = (1-\gamma_t)F_{3,j_s,t}^{s}$), it was found that the performance of the optimization algorithm is worsened significantly when adding such constraints. This is in agreement with the recent work of Karia et al. [5] who found that appending structurally redundant quadratic constraints worsened solver performance of mixed-integer quadratically-constrained programs for a variety of global solvers.

The following equations are used to model the reactions in the solid phase ($CaCO_3$ <-> CaO + $CO_2$) in the calciner and carbonator:

$$F_{3,CaCO_3,t}^{s} = F_{2,CaCO_3,t}^{s} - \zeta_t^{calc} \quad t \in \{1,...,N_t\} \tag{S13}$$
$$F_{3,CaO,t}^{s} = F_{2,CaO,t}^{s} + \zeta_t^{calc} \quad t \in \{1,...,N_t\} \tag{S14}$$
$$F_{6,CaCO_3,t}^{s} = F_{5,CaCO_3,t}^{s} + \zeta_t^{carb} \quad t \in \{1,...,N_t\} \tag{S15}$$
$$F_{6,CaO,t}^{s} = F_{5,CaO,t}^{s} - \zeta_t^{carb} \quad t \in \{1,...,N_t\}, \tag{S16}$$

Where $\zeta_t^{calc}$ and $\zeta_t^{carb}$ are the extent of reaction in the calciner and the carbonator respectively. These are written in terms of the reactant conversions,

$$\zeta_t^{calc} = X^{calc} F_{2,CaCO_3,t}^{s} \quad t \in \{1,...,N_t\} \tag{S17}$$
$$\zeta_t^{carb} = \bar{X}_t^{carb} F_{5,CaO,t}^{s} \quad t \in \{1,...,N_t\} \tag{S18}$$

We assume complete conversion in the calciner ($X^{calc} = 1$). This removes a bilinear term in equation S12 since $F_{5,CaCO_3,t}^{s} = \gamma_t F_{3,CaCO_3,t}^{s}$ becomes redundant when $F_{3,CaCO_3,t}^{s} = 0$. The average conversion in the carbonator is given by

$$\bar{X}_t^{carb}(1 - f_m\gamma_t) = (1-\gamma_t)f_m(1-f_w) + f_w(1-f_m\gamma_t) \quad t \in \{1,...,N_t\} \tag{S19}$$

Where $f_m$ and $f_w$ are parameters determined from experimental data [1]. The derivation of this equation is described in detail in section S3.

### S1.3 Gas/Liquid streams

The gas streams before the membrane unit and their components are modeled as

$$i_{gl} = \{7,8,9,10,11,12,13,14,15,16\} \tag{S20}$$
$$j_{gl} = \{CO_2, N_2, H_2O, O_2, CH_4\} \tag{S21}$$
$$F_{i_{gl},t}^{tot,gl} = \sum_{j \in j_{gl}} F_{i,j,t}^{gl} \quad t \in \{1,...,N_t\} \tag{S22}$$

$$z^{gl}_{i_{gl},j_{gl},t} = \frac{F^{gl}_{i_{gl},j_{gl},t}}{F^{tot,gl}_{i_{gl},t}} \quad t \in \{1,...,N_t\} \tag{S23}$$

(S24)

where we have assumed that the $CO_2, N_2, H_2O, O_2$ and $CH_4$ are the only major components. A splitter is modeled to determine how much flue gas to send to the calciner or carbonator. Since the flue gas composition does not change, it can be modelled using a single bilinear term

$$F^{gl}_{7,j,t} = F^{gl}_{8,j,t} + F^{gl}_{9,j,t} \quad j \in \quad j_{gl} \quad t \in \{1,...,N_t\} \tag{S25}$$

$$F^{gl}_{9,CO2,t} = \phi_t F^{gl}_{7,CO2,t} \quad \phi \in [0,1] \quad t \in \{1,...,N_t\} \tag{S26}$$

$$F^{gl}_{j,O_2,t} = z^{gl}_{j,O_2} F^{tot,gl}_{j,t} \quad j \in \{8,9\} \quad t \in \{1,...,N_t\} \tag{S27}$$

$$F^{gl}_{j,H2O,t} = z^{gl}_{j,H_2O} F^{tot,gl}_{j,t} \quad j \in \{8,9\} \quad t \in \{1,...,N_t\} \tag{S28}$$

$$F^{gl}_{j,N2,t} = z^{gl}_{j,N_2} F^{tot,gl}_{j,t}, \quad j \in \{8,9\} \quad t \in \{1,...,N_t\} \tag{S29}$$

where $\phi$ is the split fraction sent to the carbonator, and $z^{gl}_{j,O_2}$, $z^{gl}_{j,H_2O}$, $z^{gl}_{j,N_2}$ are fixed compositions of the NGCC flue gas. The mole balance around the calciner unit is given by

$$\zeta^{comb}_t = F^{gl}_{13,CH_4,t} \quad t \in \{1,...,N_t\} \tag{S30}$$

$$F^{gl}_{14,CH_4,t} = F^{gl}_{13,CH_4,t} - \zeta^{comb}_t \quad t \in \{1,...,N_t\} \tag{S31}$$

$$F^{gl}_{14,O_2,t} = F^{gl}_{8,O_2,t} + F^{gl}_{11,O_2,t} + F^{gl}_{12,O_2,t} - 2\zeta^{comb}_t \quad t \in \{1,...,N_t\} \tag{S32}$$

$$F^{gl}_{14,CO_2,t} = F^{gl}_{8,CO_2,t} + \zeta^{comb}_t + \zeta^{calc}_t \quad t \in \{1,...,N_t\} \tag{S33}$$

$$F^{gl}_{14,H_2O,t} = F^{gl}_{8,H_2O,t} + 2\zeta^{comb}_t \quad t \in \{1,...,N_t\} \tag{S34}$$

$$F^{gl}_{14,N_2,t} = F^{gl}_{8,N_2,t} + F^{gl}_{11,N_2,t} + F^{gl}_{12,N_2,t} \quad t \in \{1,...,N_t\}, \tag{S35}$$

where we have assumed complete combustion of natural gas (i.e., Equation S31 = 0). The oxygen requirement is determined by specifying a fixed amount of excess oxygen:

$$F^{gl}_{8,O_2,t} + F^{gl}_{11,O_2,t} + F^{gl}_{12,O_2,t} = (1 + c^{excess_{O_2}})(2\zeta^{comb}_t) \quad t \in \{1,...,N_t\}. \tag{S36}$$

The mole fraction of oxygen fed to the calciner has an upper bound specified by the rotary kiln vendor to limit the flame temperature, this specification is ensured by adding the inequality

$$\sum_{i \in \{8,11,12,13\}} F^{gl}_{i,O_2,t} \leq z^{max,calciner}_{O_2} \sum_{i \in \{8,11,12,13\}} F^{tot,gl}_{i,t} \quad t \in \{1,...,N_t\}, \tag{S37}$$

where $z^{max,calciner}_{O_2}$ is the upper limit on the $O_2$ mole fraction. The mass balance around the carbonator is given by the following equations

$$F^{gl}_{10,j,t} = F^{gl}_{9,j,t} \quad j \in O_2, H_2O, CH_4 \quad t \in \{1,...,N_t\} \tag{S38}$$

$$F^{gl}_{10,N_2,t} = F^{gl}_{9,N_2,t} + F^{gl}_{23,N_2,t} \quad t \in \{1,...,N_t\} \tag{S39}$$

$$F^{gl}_{10,CO_2,t} = F^{gl}_{9,CO_2,t} + F^{gl}_{23,CO_2,t} - \zeta^{carb}_t \quad t \in \{1,...,N_t\} \tag{S40}$$

$$F^{gl}_{10,CO_2,t} = (1 - X^{carb,CO_2})(F^{gl}_{9,CO_2,t} + F^{gl}_{23,CO_2,t}) \quad t \in \{1,...,N_t\}, \tag{S41}$$

where $X^{carb,CO_2}$ is the fractional conversion of total $CO_2$ entering the carbonator. The calciner off gas is quenched before entering the HRSG, then dried

$$F^{gl}_{15,j,t} = F^{gl}_{14,j,t} \quad j \in \{O_2, CH_4, CO_2, N_2\} \quad t \in \{1,...,N_t\} \tag{S42}$$

$$F^{gl}_{15,H_2O,t} = F^{gl}_{14,H_2O,t} + c^{quench} F^{tot,gl}_{14,t} \quad t \in \{1,...,N_t\} \tag{S43}$$

$$F^{gl}_{16,j,t} = F^{gl}_{15,j,t} \quad j \in \{O_2, CH_4, CO_2, N_2\} \quad t \in \{1,...,N_t\} \tag{S44}$$

$$F^{gl}_{16,H_2O,t} = c^{waterremoval} F^{gl}_{15,H_2O,t} \quad t \in \{1,...,N_t\}, \tag{S45}$$

where $c^{quench}$ and $c^{dryer,knockout}$ are linear coefficients determined from sensitivity analyses carried out on the Aspen model. Before the membrane compression stage, $CH_4$,$H_2O$ and $O_2$ are reduced to trace amounts. Thus, only the binary mixture of $CO_2$ and $N_2$ are considered for streams 17-24.

$$i_b = \{17, 18, 19, 20, 21, 22, 23, 24\} \tag{S46}$$

$$j_b = \{CO_2, N_2\} \tag{S47}$$

$$F^{tot,b}_{i_b,t} = \sum_{j_b} F^b_{i_b,j_b,t} \quad t \in \{1,...,N_t\} \tag{S48}$$

$$F^b_{17,j_b,t} = F^b_{16,j,t} \quad t \in \{1,...,N_t\} \tag{S49}$$

$$z^b_{i_b,j_b,t} = \frac{F^b_{i_b,j_b,t}}{F^{tot,b}_{i_b,t}} \quad t \in \{1,...,N_t\} \tag{S50}$$

The mole balance around the membrane is given by:

$$F^b_{17,j_b,t} = F^b_{18,j_b,t} + F^b_{19,j_b,t} \quad t \in \{1,...,N_t\} \tag{S51}$$

The compositions of the permeate and retentate streams are given by

$$y_{f,CO_2,t} = z^b_{17,CO_2,t} \quad t \in \{1,...,N_t\} \tag{S52}$$

$$\bar{\sigma}_t = \frac{Perm_{CO_2} A}{F^{tot,b}_{17,t}} \quad t \in \{1,...,N_t\} \tag{S53}$$

$$y_{CO_2,p,t} = z^b_{19,CO_2,t} = f(\bar{\sigma}, P_t, y_{f,CO_2}) \quad t \in \{1,...,N_t\} \tag{S54}$$

$$y_{CO_2,r,t} = z^b_{18,CO_2,t} = g(\bar{\sigma}, P_t, y_{f,CO_2,t}) \quad t \in \{1,...,N_t\} \tag{S55}$$

$$F^b_{19,CO_2,t} = y_{CO_2,p,t} F^{tot,b}_{19,t} \quad t \in \{1,...,N_t\} \tag{S56}$$

$$F^b_{18,CO_2,t} = y_{CO_2,r,t} F^{tot,b}_{18,t} \quad t \in \{1,...,N_t\} \tag{S57}$$

Where functions $f$ and $g$ are determined from the surrogate model development procedure described in section S5, and $y_{CO_2,p,t}$, $y_{CO_2,r,t}$ are the $CO_2$ mole fractions in the permeate and retentate streams respectively . The overall component balance around the CPU unit is given by

$$F^b_{19,j_b,t} = F^b_{20,j_b,t} + F^b_{21,j_b,t} \quad t \in \{1,...,N_t\}. \tag{S58}$$

A design specification on the purity of the exported $CO_2$ steam is imposed

$$F^b_{21,CO_2,t} = c^{z^{21}_{CO_2}} F^{tot,b}_{21,t} \quad t \in \{1,...,N_t\}, \tag{S59}$$

where $c^{z^{21}_{CO_2}}$ is the the $CO_2$ purity. The total flow rate of high purity $CO_2$ sent to sequestration is given by

$$F^{tot,b}_{21,t} = c^b_{19,CO_2} F^b_{19,CO_2,t} + c^{tot,b}_{19,CO_2} F^{tot,b}_{19,t} \quad t \in \{1,...,N_t\}, \tag{S60}$$

where $c^b_{19,CO_2}$ and $c^{tot,b}_{19,CO_2}$ are coefficients determined via linear regression to the output of the Aspen Plus model simulations for a range of permeate flowrate and compositions. Due to imperfect separation of $CO_2$ in the membrane and CPU units, the retentate and top-product of the CPU distillation column are mixed and portion of these gases are recycled to the carbonator:

$$F^b_{22,j_b,t} = F^b_{18,j_b,t} + F^b_{20,j_b,t} \quad t \in \{1,...,N_t\} \tag{S61}$$

$$F^b_{22,j_b,t} = F^b_{23,j_b,t} + F^b_{24,j_b,t} \quad t \in \{1,...,N_t\} \tag{S62}$$

$$F^b_{23,j_b,t} = \alpha_t F^b_{22,j_b,t} \quad \alpha_t \in [0,1] \quad t \in \{1,...,N_t\}, \tag{S63}$$

where $\alpha$ is the fraction of gases recycled to the carbonator, (the remainder 1-$\alpha$ is vented to the atmosphere).

### S1.4 DAC storage

A solids storage device before the DAC unit is modeled in order to reduce the capacity requirement of the DAC system.

$$nCaODAC_t = nCaODAC_{t-1} + F^s_{4,CaO,t} - CaO_{use} \quad t \in \{2,...,N_t\} \tag{S64}$$

$$nCaODAC_{t=1} \leq nCaODAC_{t=N_t} \tag{S65}$$

$$nCaODAC_t = nCaODAC_{t-23} \quad \text{if} \quad t(\quad \text{mod } 24) = 1, \quad t \in \{1,...,N_t\} \tag{S66}$$

Equation S64 models the accumulation of moles in the storage unit. Equation S65 limits the initial storage to be no more than the storage at the last time point. Equation S66 ensures that the amount of CaO in the storage device is the same at the start and end of each 24 hr period.

### S1.5 Heat and Work

Excess heat from the carbonator off-gas (stream 10 in Figure 1 of the main text) is used to provide heat to the dryer and HRSG. Note that the heat transfer is not depicted in the figure. Furthermore, the HRSG also has a steam cycle for power generation, as explained in detail by Sheha *et al.* [3]. In this work the HRSG and steam cycle are treated as a single unit and labelled 'HRSG'. The temperature and pressure of the inlet streams to the carbonator do not vary in temperature and pressure, however the compositions change. The outlet temperatures from the HRSG are fixed. We assume that the total enthalpies of each stream can be approximated by the pure component enthalpies (i.e., heat of mixing is neglected). The pure component enthalpies $h_{i,j}$ are taken from Aspen. An energy balance around the carbonator, dryer and HRSG gives:

$$\Delta H_t = \sum_{j\in j_{gl}} h_{9,j}F^{gl}_{9,j,t} + \sum_{j\in j_b} h_{23,j}F^{b}_{23,j,t} \tag{S67}$$

$$+ \sum_{j\in j_s} h_{5,j}F^{b}_{5,j,t} - \sum_{j\in j_s} h_{6,j}F^{b}_{6,j,t} - 3600Q^{carb,loss} \quad t\in\{1,...,N_t\} \tag{S68}$$

Where $\Delta H_t$ is enthalpy change between the carbonator off-gases (stream 10 in Figure 1 of the main text) and the vented gas from the HRSG and $h_{i,j}$ is the pure component enthalpy for stream $i$ and component $j$. The heat requirement for the dryer is determined from the inlet flowrate of water:

$$Q^{dryer}_t = c^{Qdryer}F^{gl}_{16,H_2O,t} \quad t\in\{1,...,N_t\} \tag{S69}$$

The calciner off-gases (stream 14) are quenched to 620 $^\circ$ C (stream 15) before the HRSG and exit the HRSG (stream 16) at 180°C. For a complete description of the various operating conditions and design specifications the reader is referred to the work of Sheha *et al.* [3]. The HRSG power can then be determined by the following equation

$$3600(W^{HRSG}_t + Q^{dryer}_t) = c^{\eta^{HRSG}}((c^{T_{15}} - c^{T_{16}})\bar{C}_p F^{tot,gl}_{15,t} + \Delta H_t) \quad t\in\{1,...,N_t\}, \tag{S70}$$

where $c^{\eta^{HRSG}}$ relates the heat transferred for steam generation and power produced from the HRSG, and is determined from the Aspen simulation. The cooling duty requirement for the power plant and CPU system are given as a function of stream 7 and stream 14 as follows:

$$Cduty^{PP}_t = c^{Cduty,PP}F^{tot,gl}_{7,t} \quad t\in\{1,...,N_t\} \tag{S71}$$

$$Cduty^{Carbon8}_t = c^{Cduty,Carbon8}F^{tot,gl}_{14,t} \quad t\in\{1,...,N_t\} \tag{S72}$$

The following expressions are used to compute the power requirements for the VPSA, CPU and DAC units.

$$W^{VPSA}_t = c^{WVPSA}F^{tot,gl}_{11,t} \quad t\in\{1,...,N_t\} \tag{S73}$$

$$W^{CPU}_t = c^{WCPU}F^{tot,b}_{19,t} \quad t\in\{1,...,N_t\} \tag{S74}$$

$$W^{DAC} = c^{WDAC}CaO_{use} \tag{S75}$$

The compressor before the membrane is modeled in the Aspen model with 8 stages and inter-stage cooling. We approximate the compression work using the equation for isothermal compression of an ideal gas, and scale the equation to match the compression work given by the Aspen simulation.

$$W^{Compressor}_t = c^{comp}Rc^{T_{16}}\log(P_t/c^{P_0})/3600 \quad t\in\{1,...,N_t\} \tag{S76}$$

A linear regression is performed to approximate $\ln P_t$, with coefficients shown in Table S2.

$$\ln P_t = c^{lnP}_1 P_t + c^{lnP}_2 \quad t\in\{1,...,N_t\} \tag{S77}$$

To determine a relationship between the calciner solids inputs, fuel and oxygen requirements, a correlation was developed, determined by conducting sensitivity analyses on the Aspen model. Since all relevant streams are at a fixed temperature, the following linear correlation approximates the energy balance around the calciner

$$c^{tot,gl}_{11}F^{tot,gl}_{11,t} + c^{tot,gl}_{8}F^{tot,gl}_{8,t} + c^{tot,gl}_{12}F^{tot,gl}_{12,t} \tag{S78}$$

$$= c^{s}_{1}F^{tot,s}_{1,t} + c^{s}_{6,CaCO_3}F^{s}_{6,CaCO3,t} + c^{s}_{6,CaO}F^{s}_{6,CaO,t} \quad t\in\{1,...,N_t\}. \tag{S79}$$

### S1.6 Variable bounds

Variables are bounded according to their context, e.g., flow rates are defined as positive reals and split fractions are constrained between 0 and 1. In Table S3 we show the additional variable bounds that are added to ensure that the optimization problem is bounded and that practical solutions are obtained. Other variables are bounded implicitly from the process constraints.

### S1.7 Feed compositions

As evidenced from the Aspen model of the NGCC plant[3], the composition of the flue gas (stream 7) does not change significantly with loading within the range of stable operation. The compositions of the other inlet streams are also invariant with time (streams 1,11,12 and 13). The inlet compositions are therefore fixed as parameters in the model, and are detailed in table S2.

**Table S3** Variable bounds used in the optimization model.

| Variable | Definition | Units | Lower Bound | Upper bound |
|---|---|---|---|---|
| $W_t^{PP}$ | Net power output from NGCC | GWh | 0 | $W^{PP,CAP}$ |
| $y_{CO_2,p}$ | $CO_2$ mole fraction in membrane permeate | - | 0.55 | 0.9 |
| $y_{CO_2,r}$ | $CO_2$ mole fraction in membrane retentate | - | 0 | 0.25 |
| $y_{CO_2,f}$ | $CO_2$ mole fraction in membrane feed | - | 0.3 | 0.55 |
| $\bar{\sigma}$ | Dimensionless membrane area divided by feed pressure | - | 15 | 50 |
| $flowRatio_u$ | Ratio of capacity flow to that of the base case[3] | - | 0 | 5 |
| $P_t$ | Membrane feed and retentate pressure | bar | 3 | 10 |
| $F_{2,t}^{tot,s}$ | Total solids to calciner | MMol/hr | 0 | 17 |

**Table S4** Parameters used in the CAPEX calculation. Cost Coeff ($c_u$) refers to the cost of unit $u$ with base flow $bf_u$. base Case Flow ($bcf_u$) is the flowrate provided in the paper of Sheha *et al.*[3]. Cost exponent ($e_u$) is the exponent used in cost estimation function (Equation S93).

| **Unit ($u$)** | **Cost Coeff ($c_u$) ($M)** | **base Flow ($bf_u$)** | **base Case Flow ($bcf_u$)** | **cost exponent ($e_u$)** |
|---|---|---|---|---|
| Calciner | 29.4 | 0.398 Mmol/hr | 17.061 Mmol/hr | 0.8 |
| Carbonator | 21.6 | 0.862 Mmol/hr | 13.62 Mmol/hr | 0.8 |
| DAC | 131.9 | 3.4 Mmol/hr5 | 3.42 Mmol/hr | 1 |
| HRSG, turbines+generators | 73.2 | 0.263 GW | 0.138 GW | 0.8 |
| HRSG, ductwork+stack | 105.1 | 0.110 GW | 0.109 GW | 0.9 |
| Membrane Compressor | 167.2 | 0.087 GW | 0.0559 GW | 0.75 |
| Limestone Mill | 8.08 | 0.38 Mmol/hr | 3.414 Mmol/hr | 0.7 |
| Blower | 68.7 | 42.91 Mmol/hr | 42.91 Mmol/hr | 0.75 |
| CPU | 173.1 | 40.35 Mmol/hr | 18 Mmol/hr | 0.75 |
| VPSA | 345.1 | 9.43 Mmol/hr | 5.918 Mmol/hr | 0.75 |
| BOP Cooling Water | 36.3 | 0.397 GW | 1.241 GW | 0.6 |
| BOP Feed Water | 95.0 | 0.397 GW | 0.397 GW | 1 |
| Power Plant | 567.0 | 0.74 GW | 0.74 GW | 1 |
| DAC storage | 9.9 | 13.4 Mmol | 13.4 Mmol | 0.7 |
| Membrane | 150 ($M/m$^2$)[6] | - | - | - |

## S2 Process Economics

### S2.1 CAPEX

Capacity variables $capFlow_u$ represent the maximum flow associated with each process unit, and are used to approximate the cost. The calciner, carbonator, limestone mill, blower and VPSA are scaled according to the total inlet molar flowrate. The maximum flow over time for is modeled by introducing inequality constraints

$$capFlow_{calciner} \geq F_{2,t}^{tot,s} \quad t \in \{1,..,N_t\} \tag{S80}$$

$$capFlow_{carbonator} \geq F_{5,t}^{tot,s} \quad t \in \{1,..,N_t\} \tag{S81}$$

$$capFlow_{LimestoneMill} \geq F_{1,t}^{tot,s} \quad t \in \{1,..,N_t\} \tag{S82}$$

$$capFlow_{Blower} \geq F_{16,t}^{tot,gl} \quad t \in \{1,..,N_t\} \tag{S83}$$

$$capFlow_{VPSA} \geq F_{11,t}^{tot,gl} \quad t \in \{1,..,N_t\} \tag{S84}$$

It is assumed that the cost of the cryogenic processing unit may be determined only as a function of the total flowrate of the permeate stream exiting the membrane.

$$capFlow_{CPU} \geq F_{19,t}^{tot,b} \quad t \in \{1,..,N_t\} \tag{S85}$$

The costs of the HRSG, membrane compressor and balance of power (BOP) scale with respect to the power and cooling duty. Note that the HRSG and steam cycle for power generation are treated as a single unit and labelled 'HRSG', since the cost of the steam cycle and HRSG both scale with the power output from the aggregated unit. Their capacity variables are defined using

$$capFlow_{HRSG,turbines+generators} \geq W_t^{HRSG} \quad t \in \{1,..,N_t\} \tag{S86}$$

$$capFlow_{HRSG,ductwork+stack} \geq W_t^{HRSG} \quad t \in \{1,..,N_t\} \tag{S87}$$

$$capFlow_{MembraneCompressor} \geq W_t^{Compressor} \quad t \in \{1,..,N_t\} \tag{S88}$$

$$capFlow_{BOPCoolingWater} \geq Cduty_t^{PP} + Cduty_t^{Carbon8} \quad t \in \{1,..,N_t\}. \tag{S89}$$

The cost of CaO storage before the DAC unit is determined from the maximum inventory level ($cap_{DACstorage}$)

$$cap_{DACstorage} \geq nCaODAC_t \quad t \in \{1,..,N_t\} \tag{S90}$$

The calciner capacity is given a suitable upper bound to limit the size of the overall system.

$$capFlow_{calciner} \leq capFlow^{max,calciner} \tag{S91}$$

The following equations are then used to determine the cost of each unit $u \in$ { Calciner, Carbonator, DAC, HRSG turbines+generators, HRSG ductwork + stack, Membrane Compressor, Limestone Mill, Blower, CPU, VPSA, BOP Cooling Water, BOP Feed Water, Power Plant, DAC storage }.

$$flowRatio_u bcf_u = capFlow_u \tag{S92}$$

$$unitCost_u \geq c_u (flowRatio_u \frac{bcf_u}{bf_u})^{e_u} \tag{S93}$$

where $bcf_u$ is the flowrate used in the work of Sheha et al[3], $bf_u$ and $c_u$ are the flow rate cost of a base unit for which the price is known to a good approximation. The cost ($c_u$) of standard units are determined using Aspen Process Economic Analyzer, and the cost of the calciner, carbonator, and DAC units are determined from specific vendor quotes. Values of $c_u$ are shown in Table S4. Note that these costs include not only the base cost for the equipment, but also direct labor, bare erect cost, Engineering, Construction Management, Home Office & Fees (Eng'g CM, H.O. & Fees) and project contingencies. The flow ratio with respect to the capacity flows in the work of[3] is used instead of the capacity flows for which we have the base cost since we do not expect the size of the units to vary significantly from this design and hence smaller bounds on $flowRatio_u$ may be used. We approximate the right hand side of equation S93 with a piecewise linear correlation with domain breakpoints $\{0, 0.1, 0.3, 0.5, 0.7, 1, 2, 3, 4, 5\}$, i.e., the maximum flowrate may vary between 0 and 5 times the flow used in the base case model. The incremental method ('INC' formulation provided by Pyomo[7,8]) is used to formulate a piecewize linear approximation of the nonlinear function. For the membrane unit, the cost is assumed to scale linearly with the membrane area,

$$unitCost_{membrane} \geq c_{membrane} A, \tag{S94}$$

The cost of the NGCC plant is fixed to that of a 740 MW power plant:

$$unitCost_{PowerPlant} = c_{PowerPlant}. \tag{S95}$$

Finally, the CAPEX is given by

$$CAPEX_{annualized} = CRF \sum_u unitCost_u \tag{S96}$$

where CRF corresponds to the capital recovery factor, that annualizes the capital cost based on the discount rate and lifetime reported in Table S2.

### S2.2 Operating cost (OPEX)

In this section we describe the equations used to calculate the fixed and variable OPEX of the process, with parameters shown in Table S1.

The variable OPEX expenditures are given by

$$opex_t^{CPU} = w_t EP_t W_t^{CPU} \tag{S97}$$

$$opex_t^{DAC} = w_t EP_t W^{DAC} \tag{S98}$$

$$opex_t^{Membrane} = w_t EP_t W_t^{Compressor} \tag{S99}$$

$$opex_t^{PowerPlantNG} = w_t fuelPrice F_t^{NG,PP} \tag{S100}$$

$$opex_t^{CalcinerNG} = w_t fuelPrice F_{13,t}^{tot,gl} \tag{S101}$$

$$opex_t^{VPSA} = w_t EP_t W_t^{VPSA} \tag{S102}$$

$$opex_t^{LimestonePurchase} = w_t c^{LimestonePurchase} F_{1,t}^{tot,s} \tag{S103}$$

$$opex_t^{LimestoneDisposal} = w_t c^{LimestoneDisposal} CaO_{use} \tag{S104}$$

$$opex_t^{VentedGasRecycle} = w_t CarbonPrice F_{24,CO_2,t}^{b} \tag{S105}$$

$$opex_t^{VentedGasCarbonator} = w_t CarbonPrice F_{10,CO_2,t}^{b} \tag{S106}$$

$$opex_t^{CO_2Sequestration} = c^{Sequestration} w_t F_{21,CO_2,t}^{b} \tag{S107}$$

$$opex_t^{Startup} = c^{StartUp} w_t s_t W^{PP,CAP} \tag{S108}$$

where $w_t$ are the weights for each representative time step modeled (see section S4) and are scaled such that $\sum_t w_t = 8760$ for annual operation. Summing each term over $t$ gives the annualized OPEX.

$$OPEX_{var,annual} = \sum_u \sum_t opex_t^u \tag{S109}$$

The fixed OPEX is approximated as a linear function of the total CAPEX at the aggregate level

$$OPEX_{fixed,annual} = c_1^{FixedOPEX} + c_2^{FixedOPEX} CAPEX \tag{S110}$$

The annual opex is given by

$$OPEX_{annual} = OPEX_{var,annual} + OPEX_{fixed,annual} \tag{S111}$$

The three revenue streams are from the power generation and $CO_2$ sequestration

$$revenue_t^{PowerPlant} \leq w_t EP_t W_t^{PP} \tag{S112}$$

$$revenue_t^{HRSG} \leq w_t EP_t W_t^{HRSG} \tag{S113}$$

$$revenue_t^{DAC} \leq X^{CaO,DAC} w_t CarbonPriceCaO_{use} \tag{S114}$$

$$REVENUE_{annual} = \sum_u \sum_t revenue_t^u \tag{S115}$$

### S2.3 Objective Function

The objective function is to maximize the net present value (NPV), which is given by

$$NPV(\$M) = \frac{-CAPEX_{annualized} + (REVENUE_{annual} - OPEX_{annual})}{CRF}. \tag{S116}$$

## S3 Carbonator Conversion

Here we derive a relationship between the amount of CaO recycled in the calcium looping process and the CaO conversion in the carbonator. This is motivated by the fact that the sorbent capacity of a CaO particle decreases with an increasing number of calcination and carbonation cycles. A critical assumption used in the model is that all CaO particles reach their maximum conversion in the carbonator. This provides an optimistic approximation of the conversion, but avoids needing a detailed model of the reactor. The maximum conversion of CaO for the $n^{th}$ (calcination and carbonation) cycle is given by[1]

$$X_n = f_m^n(1 - f_w) + f_w, \tag{S117}$$

with constants determined by curve fitting to experimental data. $X_n$ is the CaO conversion of the $n^{th}$ carbonation. The deactivation constant $f_m$ characterizes the decrease in reaction surface every cycle. The residual conversion, $f_w$, is the limiting conversion after a large number of cycles (e.g., 30). Summing equation S117 over $n$ and applying the appropriate weights $z(n,\gamma_t)$ (fractions of particles undergoing carbonation at cycle number $n$ ) we obtain the average conversion as a function of the split fraction $\gamma$:

$$\begin{aligned} \bar{X}(\gamma_t) &= \lim_{N\to\infty} \sum_{n=1}^{N} X_n z(n,\gamma_t) \\ &= \lim_{N\to\infty} \frac{1-\gamma_t}{1-\gamma^N} \sum_{n=1}^{N} (f_m^n(1-f_w) + f_w)\gamma_t^{n-1} \\ &= \frac{(1-\gamma_t)f_m(1-f_w)}{1-f_m\gamma_t} + f_w \end{aligned} \tag{S118}$$

Where $z(n,\gamma_t)$ is the fraction of particles undergoing carbonation at cycle number $n$. By multiplying through by $(1-f_m\gamma_t)$ we obtain a constraint involving only bilinear terms that is used in the optimization model along with equation S18. In Figure S1 we show the conversion per pass ($\bar{X_n}$) and the mole fraction of particles entering each cycle ($z$). The conversion decreases rapidly at first with increasing cycle number and reaches the residual conversion $f_w$ asymptotically. The smaller the split fraction, the more the particle distribution is shifted to lower cycle numbers. The particle fraction decreases more rapidly with $n$ at lower values of $\gamma$. Specific values of $f_m$ and $f_w$ are chosen to match an operating point given by the carbonator vendor (average conversion of 0.65 at a split fraction $\gamma = 0.5$), and correspond to the correlated data of[1] for Purbeck limestone calcined at 1023 K and particle size between 850 and 1000 $\mu$m.

In Figure S2 we show the average conversion for various values of the split fraction. As the split fraction approaches 1, all particles are recycled infinitely and the average conversion approaches $f_w$, implying that it may be possible to operate without any fresh feed at the expense of lower conversion per cycle. There are therefore feasible solutions to the optimization model where the limestone milling and DAC units are not built, but the calcium loop and downstream separations units are built similar to a standard calcium-looping carbon capture process without DAC, with full recycle of the calcined solids to the carbonator.

## S4 Reducing the number of discrete time points

The k-means clustering algorithm used to determine representative days and their corresponding weights is described in in Algorithm 7.

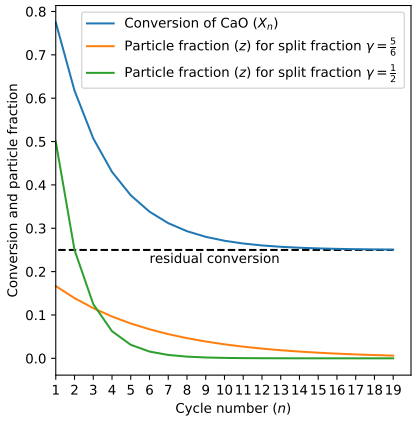


**Figure S1** Figure to show the terms in equation S118 for various values of $n$ with $f_m = 0.7$ and $f_w = 0.25$[1].

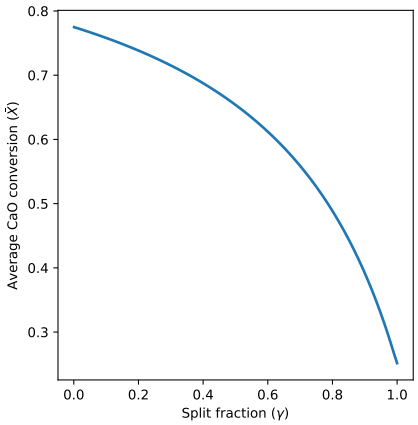


**Figure S2** Modeled average CaO conversion as a function of solids split fraction $\gamma$, for Purbeck limestone with diameter 850-1000 micrometers[1].

## S5 Membrane surrogate model

The process consists of a single-stage membrane that is used to purify the gas stream to a suitable level before the cryogenic processing unit. In previous work[3], a model for the membrane was developed that uses the cross-plug flow assumption and determines the compositions and flowrates of the permeate and retentate as a function of the design and operational degrees of freedom, namely the membrane area, $A$, the flow rate and composition of the feed to the membrane (stream 17), and the feed pressure ($P_t$). It is assumed that there is no pressure drop on the retentate side, the process is isothermal, and the pressure of the permeate stream is fixed to 1 bar. Furthermore, since all components other than $CO_2$ and $N_2$ are reduced to trace amounts before the membrane module, only the binary mixture of $CO_2$ and $N_2$ is considered. The key operational degree of freedom is the feed pressure ($P_t$), which is allowed to vary with time in response to varying feed conditions. In Figure S6 we show a schematic of the membrane model.

The cross-plug flow model may be written as an ordinary differential equation in terms of dimensionless quantities as follows[9]. Introducing the dimensionless quantities:

$$\pi = \frac{Perm_{CO_2}}{Perm_{N_2}} \tag{S119}$$

$$\kappa = \frac{P_p}{P} \tag{S120}$$

$$\theta = \frac{F_{19}^{tot,b}}{F_{17}^{tot,b}} \tag{S121}$$

$$\omega = \frac{F_{18}^{tot,b}}{F_{17}^{tot,b}} \tag{S122}$$

$$\sigma = \frac{Perm_{CO_2} PA}{F_{17}^{tot,b}} \tag{S123}$$

Where $\pi$ is the ratio of $CO_2$ permeance to $N_2$ permeance, $\theta$ is the stage cut, $\omega = 1 - \theta$, and $\sigma$ is the dimensionless membrane area. The

**Algorithm 1** Algorithm used to reduce the number of discrete time points

**input:**

- Electricity price profile $EP_t^*$, $t \in [1,...,N_t]$, ($N_t$ default 8760)
- Number of hours in a representative period, $N_p$ (default 24)
- Number of clusters, $N_c$ (default 30)
- Number of centroid seeds $N_s$ (default 1000)

**output:**

- New electricity price profile $EP_t$.
- Vector of corresponding weights $w_t$

**begin**

1. Split $EP_t$ into consecutive periods of length $N_p$. If $N_t \mod N_p \neq 0$ then remove the trailing days.

2. Determine $N_c$ centroids and their corresponding weights $w_t$ using k-means clustering (scikitlearn KMeans algorithm) with $N_s$ random seeds.

3. For each centroid returned by the k-means algorithm, determine the period from the original profile that minimizes the L2 norm between that period and the centroid.

4. Scale the weights such that $\sum_t w_t EP_t = \sum_t EP_t^*$, i.e., the approximate profile has the same average price as the true profile.

**end**

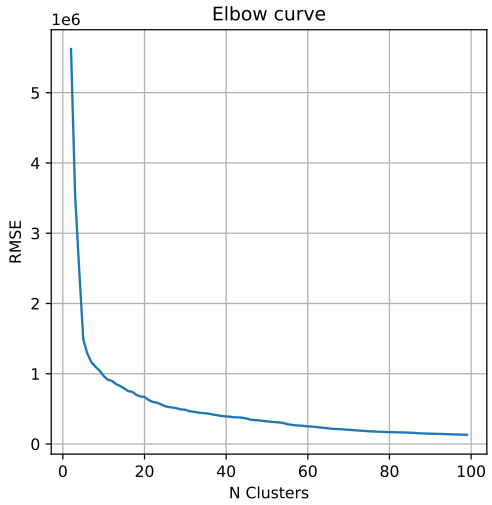


**Figure S3** Root mean squared error (RMSE) vs the number of clusters $Nc$ (or representative days) for the MiNg $150 PJM electricity price scenario.

ODE relating $y_{CO_2,r}$ with $\sigma$ is given by

$$\frac{dy_{CO_2,r}}{d\sigma} = \frac{(y_{CO_2,r} - y'_{CO_2,p})(y_{CO_2,r} - \kappa y'_{CO_2,p})}{y'_{CO_2,p}\omega}. \tag{S124}$$

$y'_{CO_2,p}$ is the local composition of $CO_2$ in the permeate stream. The ODE relating $\omega$ with $\sigma$ is given by

$$\frac{d\omega}{d\sigma} = -\frac{y_{CO_2,r} - \kappa y'_{CO_2,p}}{y'_{CO_2,p}}. \tag{S125}$$

$$y'_{CO_2,p} = \frac{1 + (\pi - 1)(\kappa + y_{CO_2,r}) - \sqrt{[1 + (\pi - 1)(\kappa + y_{CO_2,r})]^2 - 4\pi\kappa(\pi - 1)y_{CO_2,r}}}{2\beta(\pi - 1)} \tag{S126}$$

After integrating equations S124,S125 and S126 the $CO_2$ purity in the permeate can be expressed as

$$y_{CO_2,p} = \frac{y_{CO_2,f} - \omega(\sigma^{final})y_{CO_2,r}(A)}{1 - \omega(\sigma^{final})}, \tag{S127}$$

Where $\sigma^{final}$ is the upper limit of integration of the dimensionless membrane area and $\omega(\sigma^{final})$ is the ratio of the retentate flow rate to the feed flow rate evaluated at the final coordinate of integration. The initial conditions are given by

$$y_{CO_2,r}(\sigma = 0) = y_{CO_2,f} \tag{S128}$$

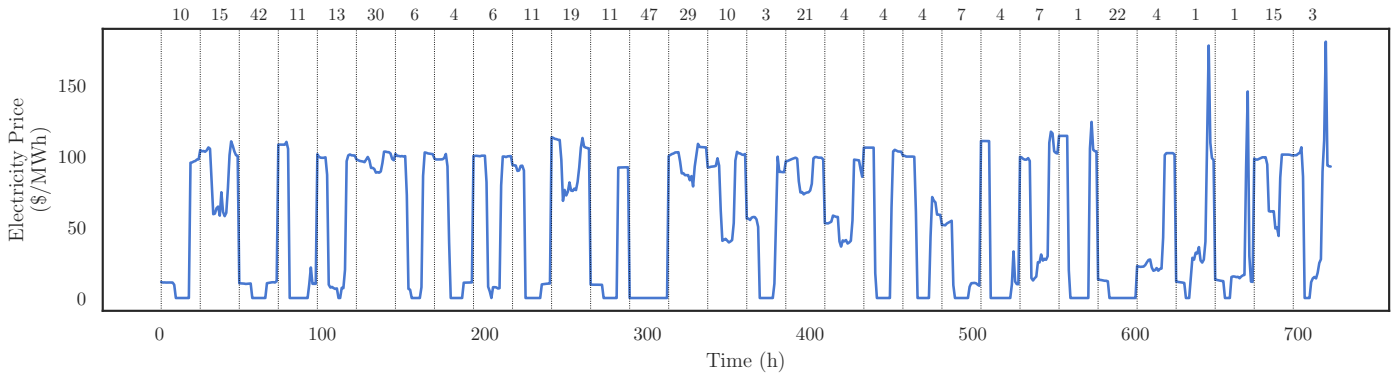


**Figure S4** Electricity price profile used to represent the MiNg $150 electricity price scenario. The dotted lines represent the boundary between each characteristic day. The numbers at the top are the corresponding weights $w_t$ that are assigned to each hour in the price profile.

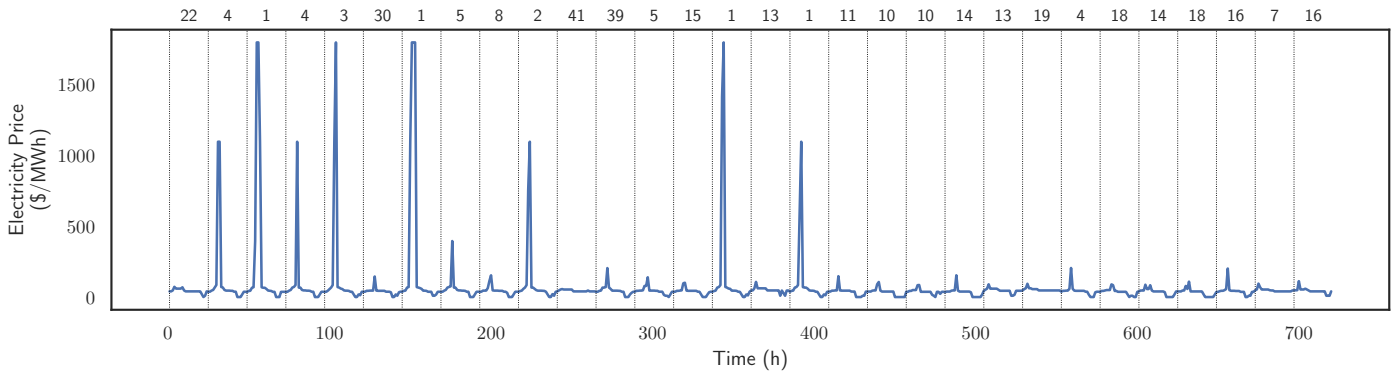


**Figure S5** Electricity price profile used to represent the BaseCaseTax electricity price scenario. The dotted lines represent the boundary between each characteristic day. The numbers at the top are the corresponding weights $w_t$ that are assigned to each hour in the price profile.

$$\omega(\sigma = 0) = 1 \tag{S129}$$

The permeance values of $CO_2$ ($Perm_{CO_2}$) and $N_2$ ($Perm_{N_2}$) are shown in table S1 and reflect the performance of a commercially available membrane[6].

Since representation of the explicit solutions from the ODE in an optimization model is computationally expensive, we developed reduced order functions that approximate the solution to the ODE in the optimization model. In addition to the overall component mass balances (equation S51), two more equations are required to fully specify the membrane unit. We choose to determine functions $f$ and $g$ for the $CO_2$ mole fractions in the permeate and retentate streams. $\bar{\sigma}$, $P$ and $y_{f,CO_2}$ are chosen as the independent variables, where $\bar{\sigma} = \sigma/P$:

$$y_{CO_2,p} = f(\bar{\sigma}, P, y_{CO_2,f}) \tag{S130}$$

$$y_{CO_2,r} = g(\bar{\sigma}, P, y_{CO_2,f}) \tag{S131}$$

Suitable bounds for the independent variables are chosen as $\bar{\sigma} \in [15,50]$, $P \in [3,10]$, $y_{f,CO_2} \in [0.3,0.55]$. The reduced-order functions are generated using the ALAMO software[10]. The adaptive sampling functionality is employed in order to avoid over-fitting of the model outputs. Bounds on $y_{CO_2,p}$ and $y_{CO_2,r}$ are set to between 0 and 1 to ensure that the resulting model is physical over the domain of input variables. The AICc (corrected Akaike's information criterion) is used as the fitness metric. This rewards goodness of fit and includes a penalty that increases with the number of estimated parameters, resulting in a simpler surrogate model. The following basis functions are specified: monomial power coefficients (-1,0.5,1,2), powers of two terms (1,2), powers of three terms (1), linear functions and a constant. These basis functions are used so that the resultant model does not introduce too many bilinear or quadratic terms when reformulated for the optimization model. The equations that minimize the AICc metric are:

$$y_{CO_2,r} = c_1^{surr}\bar{\sigma} + c_2^{surr}\bar{\sigma}^2 + c_3^{surr} \tag{S132}$$

$$y_{CO_2,p} = c_4^{surr}\bar{\sigma} + c_5^{surr}P + c_6^{surr}y_{f,CO_2} + c_7^{surr}y_{f,CO_2}^2 \tag{S133}$$

The $R^2$ values for $y_{CO_2,r}$ and $y_{CO_2,p}$ are 0.975 and 0.981 respectively over the 100 sampled points generated during the surrogate model development routine. In Figures S7 and S8 we show the performance of the surrogate model with respect to the ODE model at various feed mole fractions and pressures.

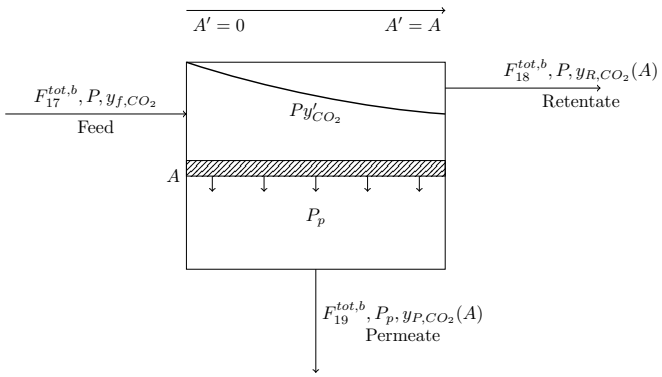


**Figure S6** Model schematic for cross- plug flow gas separation membrane based on[9]. Variables with superscript "'" represent local values (which are functions of the area coordinate). $y_{P,CO_2}(A)$ $y_{R,CO_2}(A)$ indicate the mole fractions at the end of the unit (where $A' = A$).

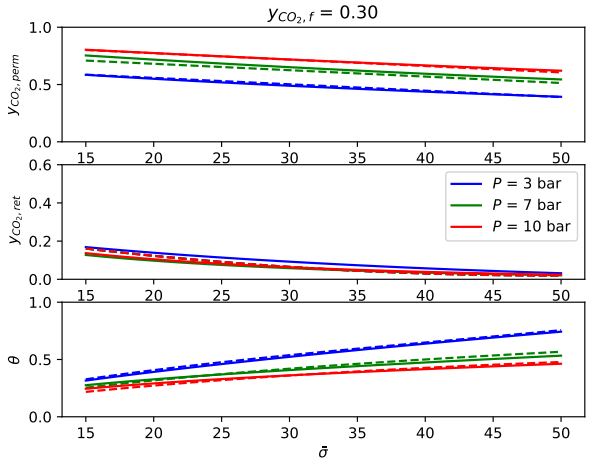


**Figure S7** Performance of the membrane surrogate model (dashed lines) with respect to the solution to the ODE model (continuous lines) at feed mole fraction $y_{CO_2,f} = 0.3$

## S6 Optimal dispatch of the coupled system at $200/ton carbon price

Figure S9 shows the NPV-optimal dispatch of the coupled system under the MiNg $150 PJM market scenario with carbon price changed to $200/tonne.

## S7 Recycling all separation gases to the carbonator

Here we consider the case where we enforce that all off-gases from the membrane (retentate) and CPU (distillation top product) are all recycled back the carbonator for further $CO_2$ capture, i.e., $\alpha_t = 1$. Operating in such a way may be desirable from an environmental standpoint if net emissions are to be minimized.

In Table S5 we summarize the key metrics for comparison. As expected, the $CO_2$ capture efficiency is higher in the case where no gases are vented before the carbonator. However, this comes at a cost of $\approx$ $150M in NPV. In Figure S10 we show a comparison of plant operation in the two cases. In the case where all gases are recycled, the solids split fraction $\gamma_t$ is higher at full loading and the CaO conversion is lower. With a fixed calciner capacity of 17 MMol/hr, the system is able to calcine more feed $CaCO_3$ in the case where we are able to vent some of the recycled gases due to the decreased CaO degradation within the carbonator. Additional benefits of relaxing the constraint on the degree of recycle are that there is less variation in the solids flowrate to the carbonator and there are less periods of part-loading operation of the NGCC plant.

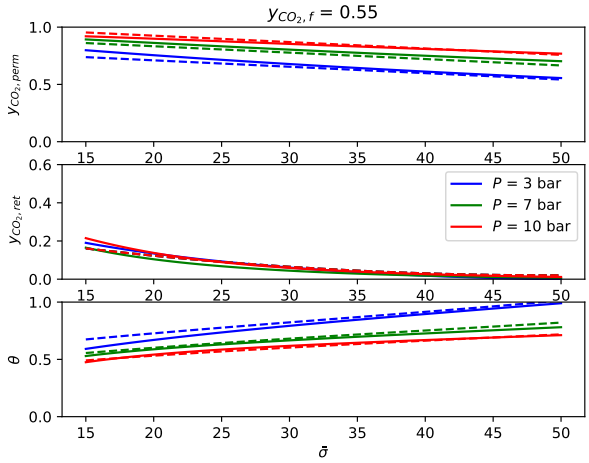


**Figure S8** Performance of the membrane surrogate model (dashed lines) with respect to the solution to the ODE model (continuous lines) at feed mole fraction $y_{CO_2,f} = 0.55$

**Table S5** Comparison of key metrics for optimal MiNg $150 PJM scenario relaxing constraint on recycle. *annual OPEX/ annual net power **annual $CO_2$ capture rate excluding DAC as a fraction of annual $CO_2$ input to the system. $CO_2$ input to the system is defined as the total $CO_2$ that enters the system, including $CO_2$ present in calcium carbonate and natural gas.

| | Units | Relax Recycle | Fix Recycle |
|---|---|---|---|
| NPV | $bn | 1.966 | 1.817 |
| Upper Bound | $bn | 1.970 | 1.830 |
| Abs. Gap | $bn | 0.004 | 0.013 |
| Rel. Gap (%) | - | 0.186 | 0.710 |
| Fraction of hours NGCC on | - | 0.516 | 0.515 |
| NGCC power | TWh/yr | 3.286 | 3.264 |
| Net power | TWh/yr | 2.205 | 2.303 |
| Cost of power* | $/MW | 267 | 214 |
| $CO_2$ capture efficiency** | - | 0.940 | 0.987 |
| Net $CO_2$ emissions | ton/yr | -437 | -403 |

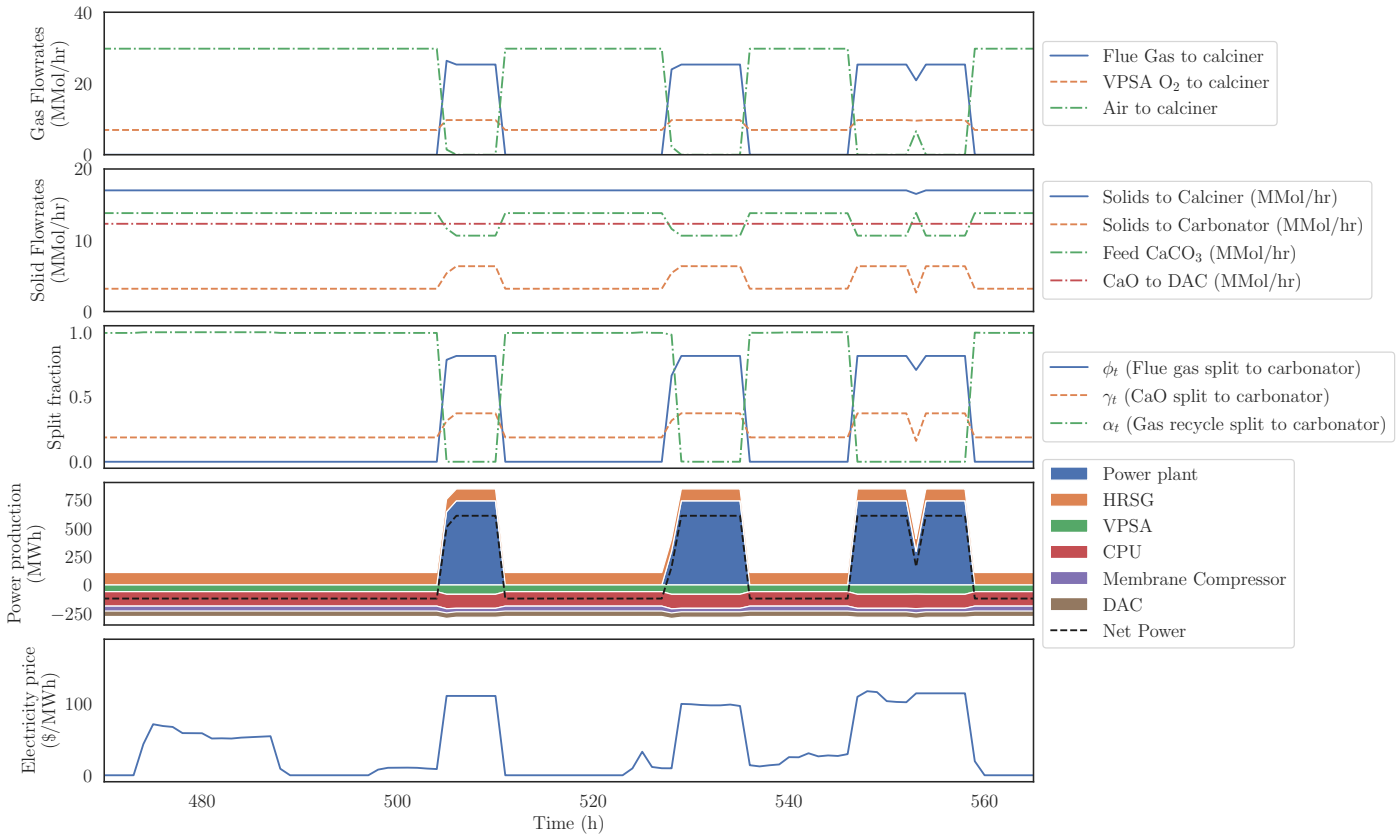


**Figure S9** Optimal dispatch of the coupled system under the MiNg $150 PJM market scenario with carbon price changed to $200/tonne.

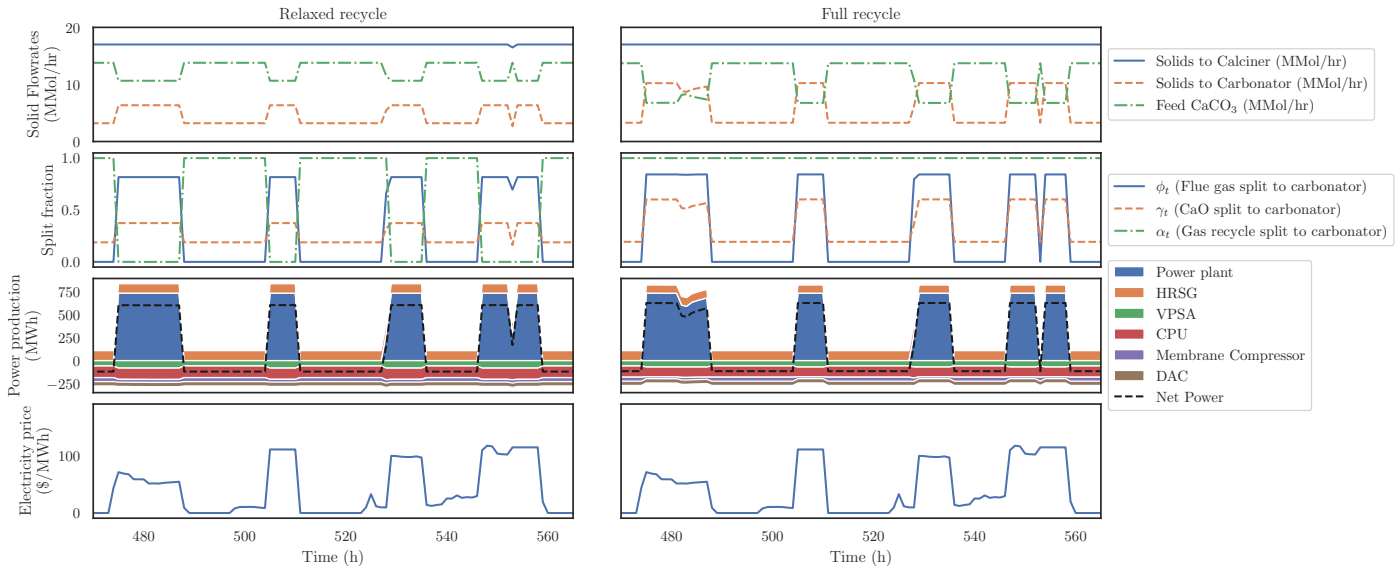


**Figure S10** Comparison of optimal dispatch under the MiNg $150 PJM market scenario. Left: the gas recycle split fraction ($\alpha_t$) is allowed to vary. Right: the gas recycle split fraction ($\alpha_t$) is fixed to 1 (all gases are recycled).

## Notes and references


[1] P. S. Fennell, R. Pacciani, J. S. Dennis, J. F. Davidson and A. N. Hayhurst, *Energy & Fuels*, 2007, **21**, 2072–2081.

[2] N. Kumar, P. Besuner, S. Lefton, D. Agan and D. Hilleman, *Power plant cycling costs*, National renewable energy lab.(nrel), golden, co (united states) technical report, 2012.

[3] M. Sheha, E. Graham, D. Mallapragada, E. Gencer, P. Cross, J. Custer, A. Goff, I. Cormier and H. Herzog, *engrXiv preprint*, 2023, DOI: 10.31224/3006.

[4] J. P. Ruiz and I. E. Grossmann, *Computers & Chemical Engineering*, 2011, **35**, 2729–2740.

[5] T. Karia, C. S. Adjiman and B. Chachuat, *Computers & Chemical Engineering*, 2022, **165**, 107909.

[6] T. Merkel, K. Amo, R. Baker, R. Daniels, B. Friat, Z. He, H. Lin and A. Serbanescu, *Membrane process to sequester CO2 from power plant flue gas*, Membrane technology & research incorporated technical report, 2009.

[7] W. E. Hart, J.-P. Watson and D. L. Woodruff, *Mathematical Programming Computation*, 2011, **3**, 219–260.

[8] M. L. Bynum, G. A. Hackebeil, W. E. Hart, C. D. Laird, B. L. Nicholson, J. D. Siirola, J.-P. Watson and D. L. Woodruff, *Pyomo–optimization modeling in python*, Springer Science & Business Media, 3rd edn, 2021, vol. 67.

[9] M. Gazzani, M. Mazzotti, F. Milella and P. Gabrielli, *ETH Zürich*, 2016.

[10] A. Cozad, N. V. Sahinidis and D. C. Miller, *AIChE Journal*, 2014, **60**, 2211–2227.